


RESEARCH

Open Access



The renoprotective efficacy and safety of genetically-engineered human bone marrow-derived mesenchymal stromal cells expressing anti-fibrotic cargo

Yifang Li^{1,3}, Alex Hunter^{1,3}, Miqdad M. Wakeel^{1,3}, Guizhi Sun^{2,4}, Ricky W. K. Lau^{2,3}, Brad R. S. Broughton^{1,3}, Ivan E. Oyarce Pino^{1,3}, Zihao Deng⁵, Tingfang Zhang^{2,3}, Padma Murthi^{1,3}, Mark P. Del Borgo^{1,3}, Robert E. Widdop^{1,3}, Jose M. Polo^{2,4,6,7}, Sharon D. Ricardo^{2,3*} and Chrishan S. Samuel^{1,2,3,8*} 

Abstract

Background Kidney fibrosis is a hallmark of chronic kidney disease (CKD) and compromises the viability of transplanted human bone marrow-derived mesenchymal stromal cells (BM-MSCs). Hence, BM-MSCs were genetically-engineered to express the anti-fibrotic and renoprotective hormone, human relaxin-2 (RLX) and green fluorescent protein (BM-MSCs-eRLX + GFP), which enabled BM-MSCs-eRLX + GFP delivery via a single intravenous injection.

Methods BM-MSCs were lentiviral-transduced with human relaxin-2 cDNA and GFP, under a eukaryotic translation elongation factor-1 α promoter (BM-MSCs-eRLX + GFP) or GFP alone (BM-MSCs-eGFP). The ability of BM-MSCs-eRLX + GFP to differentiate, proliferate, migrate, produce RLX and cytokines was evaluated in vitro, whilst BM-MSC-eRLX + GFP vs BM-MSCs-eGFP homing to the injured kidney and renoprotective effects were evaluated in preclinical models of ischemia reperfusion injury (IRI) and high salt (HS)-induced hypertensive CKD in vivo. The long-term safety of BM-MSCs-RLX + GFP was also determined 9-months after treatment cessation in vivo.

Results When cultured for 3- or 7-days in vitro, 1×10^6 BM-MSCs-eRLX + GFP produced therapeutic RLX levels, and secreted an enhanced but finely-tuned cytokine profile without compromising their proliferation or differentiation capacity compared to naïve BM-MSCs. BM-MSCs-eRLX + GFP were identified in the kidney 2-weeks post-administration and retained the therapeutic effects of RLX in vivo. $1-2 \times 10^6$ BM-MSCs-eRLX + GFP attenuated the IRI- or therapeutically abrogated the HS-induced tubular epithelial damage and interstitial fibrosis, and significantly reduced the HS-induced hypertension, glomerulosclerosis and proteinuria. This was to an equivalent extent as RLX and BM-MSCs administered separately but to a broader extent than BM-MSCs-eGFP or the angiotensin-converting enzyme inhibitor, perindopril. Additionally, these renoprotective effects of BM-MSCs-eRLX + GFP were maintained in the presence of perindopril co-treatment, highlighting their suitability as adjunct therapies to ACE inhibition. Importantly, no major long-term adverse effects of BM-MSCs-eRLX + GFP were observed.

*Correspondence:

Sharon D. Ricardo

sharon.ricardo@monash.edu

Chrishan S. Samuel

chrishan.samuel@monash.edu

Full list of author information is available at the end of the article



© The Author(s) 2024. **Open Access** This article is licensed under a Creative Commons Attribution 4.0 International License, which permits use, sharing, adaptation, distribution and reproduction in any medium or format, as long as you give appropriate credit to the original author(s) and the source, provide a link to the Creative Commons licence, and indicate if changes were made. The images or other third party material in this article are included in the article's Creative Commons licence, unless indicated otherwise in a credit line to the material. If material is not included in the article's Creative Commons licence and your intended use is not permitted by statutory regulation or exceeds the permitted use, you will need to obtain permission directly from the copyright holder. To view a copy of this licence, visit <http://creativecommons.org/licenses/by/4.0/>.

Conclusions BM-MSCs-eRLX + GFP produced greater renoprotective and therapeutic efficacy over that of BM-MSCs-eGFP or ACE inhibition, and may represent a novel and safe treatment option for acute kidney injury and hypertensive CKD.

Keywords Chronic kidney disease, Fibrosis, BM-MSCs, Relaxin, Genetic engineering

Background

Chronic kidney disease (CKD) is defined as kidney damage that occurs over at least 3 months and affects 1 in 10 of the general population worldwide [1]. Regardless of aetiology, kidney fibrosis is the final common manifestation of CKD and is the key contributor to kidney dysfunction and end-stage renal disease [2, 3]. Kidney fibrosis can manifest in the form(s) of tubulointerstitial fibrosis, glomerulosclerosis and/or vascular fibrosis, which disrupts normal kidney architecture and drives progressive cell death and irreversible kidney dysfunction [3, 4]. Despite this, there are currently no effective cures that can reverse or even reduce established fibrosis progression.

Human bone marrow-derived mesenchymal stem/stromal cells (BM-MSCs) have emerged as a novel treatment option for CKD owing to their immunomodulatory and tissue-reparative actions [5–7]. Substantial evidence has demonstrated the renoprotective effects of these non-immunogenic adult stem cells in various pre-clinical models of acute and chronic kidney injury [6], and an excellent safety profile in numerous clinical studies [8–11]. However, it has emerged that the viability of BM-MSCs post-transplantation is significantly impaired within fibrotic environments [6]. This may explain the lack of consistent efficacy of BM-MSCs in various clinical trials that have evaluated the effects of autologous or allogenic cell administration to CKD patients [8, 9]. Hence, to improve the therapeutic efficacy of BM-MSCs, various strategies have explored the genetic-engineering of cells with specific microRNAs [12], anti-inflammatory agents [13], anti-apoptotic factors [14] or angiogenic factors [15]. However, at best these strategies have had limited success in addressing the multifactorial nature of fibrosis, and do not facilitate the resolution of established fibrosis in CKD.

In light of these challenges, we have developed an innovative approach to combine BM-MSCs with recombinant human gene-2 (H2) relaxin (RLX) [6, 16], the drug-based form of H2 relaxin. The rationale for choosing RLX over other clinically-available therapies for kidney disease was based on the rapid anti-fibrotic actions it induces independently of etiology, sex or species [17–26], and over currently-used treatments for CKD [27, 28]. These effects of RLX are mediated via its

suppression of transforming growth factor (TGF)- β 1-induced myofibroblast differentiation and extracellular matrix (ECM) production, and promotion of matrix metalloproteinase (MMP)-induced ECM degradation.

The combined effects of RLX (0.5 mg/kg/day; via subcutaneous administration) and BM-MSCs (1×10^6 /mouse; via intravenous delivery ~15–30 min after RLX delivery) completely prevented tubulointerstitial fibrosis in mice with obstructive nephropathy [29], and more effectively attenuated interstitial fibrosis and glomerulosclerosis compared to the angiotensin-converting enzyme (ACE) inhibitor, perindopril, in a murine model of uninephrectomy followed by subcutaneous implantation of a deoxycorticosterone acetate pellet and saline to drink (1 K/DOCA/salt) for 3-weeks [28], after a 7-day treatment period. Additionally, BM-MSCs effectively lowered blood pressure (BP) to similar extent as perindopril in hypertensive mice [28]. These findings highlighted the enormous therapeutic potential of enhancing the immunomodulatory and anti-hypertensive effects of BM-MSCs with the anti-fibrotic actions of RLX in treating fibrotic kidney diseases.

However, a potential drawback to the clinical application of administering this combination therapy, is that each treatment would have to be administered separately; that is through daily injections or a microinfusion pump containing RLX [30] (due to its relatively short in vivo half-life of ~4–8 h [31, 32]), followed by single or multiple intravenous injections of BM-MSCs. When compared to current the standard-of-care medications that are orally consumed, this would be cumbersome and may affect patient compliance. To address this issue, we genetically-engineered and characterised BM-MSCs that expressed RLX via lentiviral transduction, to ensure constant delivery of therapeutic levels of RLX at the site of cell engraftment following transplantation. We then evaluated the anti-fibrotic and other renoprotective effects of these RLX-expressing BM-MSCs in preclinical models of acute kidney injury (which often contributes to CKD [33]) and hypertensive CKD (induced by high salt loading). In the latter model, we also compared and combined the effects of RLX-expressing BM-MSCs to that of a clinically-used frontline treatment for CKD, and evaluated the long-term safety of these engineered cells.

Methods

Materials

Recombinant H2 relaxin was generously provided by Corthera Inc. (San Carlos, CA, USA; a subsidiary of Novartis AG, Basel, Switzerland). Human BM-MSCs were commercially purchased from the Tulane Centre for Stem Cell Research and Regenerative Medicine (Tulane University, New Orleans, LA, USA; Website: <https://medicine.tulane.edu/stem-cell-research-regenerative-medicine>). Prior to any experiments being conducted on this study, these BM-MSCs were previously characterised to display a normal karyotype, form colony-forming unit-fibroblasts (CFU-F), and show multi-lineage differentiation potential [34]. These BM-MSCs were also found to express the cell surface antigens CD73, CD90 and CD105 (confirming that they were MSCs), but lacked expression of CD14, CD19, CD34, CD45 (confirming that they were not of hemopoietic or endothelial origin) and MHC class II human leukocyte antigen-DR isotype (HLA-DR; confirming that they were immunoprivileged) [34]. Perindopril Erbumine was manufactured by MedChem Express (Monmouth, NJ, USA).

Human BM-MSC culture

Human bone marrow-derived mesenchymal stem cells (BM-MSCs) were cultured in α -minimal essential media (α -MEM) supplemented with 16% fetal bovine serum (FBS), 1% L-glutamine (2 mM) and 1% penicillin/streptomycin (100U/ml) (all from Thermo Fisher Scientific, Scoresby, Victoria, Australia) at 37 °C, and were seeded at a density of 60 cells/cm² in tissue culture flasks (BD Falcon, North Ryde, New South Wales, Australia) with media replaced every 3–4-days until 70–80% confluency was reached. Passages 3–4 (P3-P4) cells were used for transduction.

Lentiviral production

To expand pLV-EF1A (eukaryotic translation elongation factor-1 α)-hRLN2-EGFP lentiviral vector DNA (Fig. 1A), ~1 mL (75 ng) of vector DNA was mixed with ~10 μ L of one-shot stb13 competent *E.coli* (C737303; Thermo Fisher Scientific, Scoresby, Victoria, Australia), and incubated for 30 min, before subjected to heat shock in a water bath for 30 s at 42 °C, and incubated on ice immediately following that. Bacteria were then transferred to 500 μ L SOC medium (15,544,034; Thermo Fisher Scientific) and shaken at 37 °C for 1 h at 225 rpm, before 250 μ L was spread onto a pre-warmed ampicillin (50 μ L/mL) LB-amp plate and incubated overnight at 37 °C. On the following day, one colony was picked into 5–7 mL LB-Amp broth to expand in a shaker (for 8 h at 225 rpm, at 37 °C), before being diluted at 1:1000 with 100 mL LB-Amp broth and incubated in 37 °C in a

shaker at 250 rpm for 16 h. The next day, plasmid DNA was extracted and purified using a QIAGEN Plasmid Plus Midi Kit (#12,943 and #12,945) following the manufacturer's protocol. The DNA concentration of the pLV-EF1A-hRLN2-EGFP and pLV-EF1A-EGFP plasmids were 1483 ng/ μ L and 553 ng/ μ L, respectively.

Lentiviral expansion and titre determination

Lentiviral particles containing pLV-EF1A-hRLN2-EGFP or pLV-EF1A-EGFP were produced in HEK293T cells by transient co-transfection using the three-plasmid expression system. Briefly, 17.5 million cells were plated into a T175 flask a day before transfection and 24 h later, the culture medium was replaced by supplemented advanced DMEM containing 2% FBS (Invitrogen, Mount Waverley, Victoria, Australia), 1% non-essential amino acids (NEAA; Sigma-Aldrich, Castle Hill, New South Wales, Australia), 1% GlutaMax (2 mM; Invitrogen, Australia) and 1% penicillin/streptomycin (100U/ml) prior to the addition of transfection mix containing transfer vector DNA (with human relaxin-2 gene), packaging plasmid DNA (psPAX2; Addgene Plasmid #12,260) and envelope plasmid DNA (pMD2.G; Addgene plasmid #12,259) at a 2.5:1.6:1 ratio in 1.25 ml of sterile H₂O per T175 flask, which contained 4.5 μ g PEI/ μ g total DNA. The medium was replaced after 16–24 h (on day-2) and again after 48 h (on day-3) post-transfection. On day-3, the conditioned medium containing the lentiviral particles was collected into sterile 50 mL tubes. To increase the viral titer, the cell culture supernatant containing lentiviral particles, at 72 h post-transfection, was filtered through a 0.45 μ m stericup-HV sterile vacuum filtration system (SCHVU01RE; Millipore Merck, Darmstadt, Germany) and transferred to Millipore concentrators with a 100 kDa cut-off (Amicon®Ultra-15, Merck Millipore, Tullagreen, Cork, Ireland) and centrifuged repeatedly for 20–30 min at 4000 rpm at 4 °C until the sample of each supernatant was concentrated to ~200 μ L. The concentrated samples containing lentiviral particles were finally transferred to 0.2 ml Eppendorf tubes and stored at -80 °C until required.

To determine the virus titre (the number of host cells per unit virus can infect), cryopreserved BM-MSCs were seeded in 12-well plates at a density of 5 \times 10⁴ cells per well. After incubation at 37 °C for 24 h, the culture medium was replaced with 0.5 mL of virus particles diluted by 1000-, 10,000- and 100,000-fold in α -MEM supplemented with 2% FBS, 1% L-glutamine (2 mM) and 1% penicillin/streptomycin (100U/ml), in the presence of polybrene transfection reagent (1:1700; TR-1003-G; EMD Millipore, Merck KGaA, Darmstadt, Germany) in duplicate. Notably, cells that were transduced with pLV-EF1A-hRLN2-EGFP and pLV-EF1A-EGFP were termed

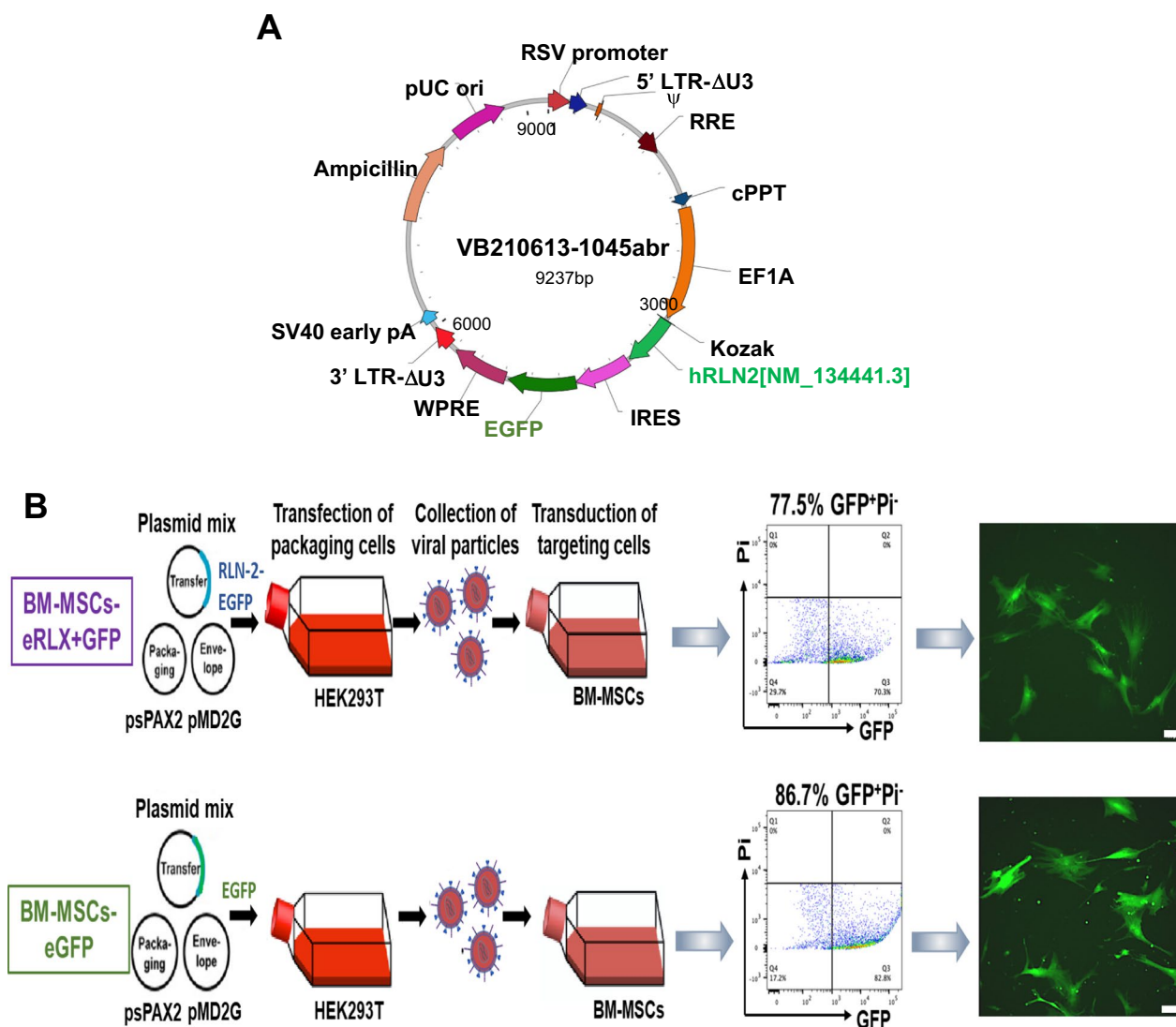


Fig. 1 Design, transduction and characterisation of BM-MSCs-eRLX + GFP. **A** Shows a schematic illustration of the pLV-EF1A-hRLN2-EGFP vector that was designed and transduced into BM-MSCs. The vector comprised bicentrically expressed human relaxin-2 cDNA and EGFP genes linked by internal ribosome entry site (IRES), under an EF1A promoter. **B** Lentivirus was produced with a three-plasmid expression system with transfer (which contained the *RLN-2-EGFP* genes or *EGFP* gene of interest), packaging and envelope plasmids in HEK293T cell lines, before being transduced into passage (P)3–4 BM-MSCs at a MOI of 2. After flow sorting, the successfully transduced cells (GFP⁺) were expanded and passaged until P6, when they were subjected to flow cytometry analysis of GFP⁺ cells to test the long-term stability of lentiviral transduction, which represented averages of ~77.5% and ~86.7% of BM-MSCs transduced with virus containing pLV-EF1A-hRLN2-EGFP or pLV-EF1A-EGFP, respectively. Representative fluorescent microscopy images also confirmed the GFP expression in the P6 BM-MSCs-eRLX + GFP and BM-MSCs-eGFP, respectively. Scale bar = 100 μm

BM-MSCs-eRLX + GFP and BM-MSCs-eGFP (as a control engineered cell type), respectively. The culture medium was replaced with 1 mL of MSC medium every 24 h. At 72 h post-transduction, transduction efficiency was measured by detecting % GFP-positive (GFP⁺) cells on a LSR Fortessa flow cytometer at a concentration of 2.5×10^5 cells/mL in FACS buffer (0.5% BSA, 0.5% 0.5 M EDTA in PBS) with propidium iodide (PI; 1:500; P4864; Sigma-Aldrich). The transduction efficiency (F) was then

used to calculate the virus titer (infectious units per μl of virus), by multiplying the number of targets MSCs (Cn), and dividing that by the volume of input virus (V).

BM-MSC transduction

Cryopreserved human BM-MSCs were plated at a density of 5×10^4 cells per well in a 12-well plate. According to the virus titre calculated using the formula described above (1.58×10^7 TU/ml and 1.5×10^8 TU/ml for Lentiviral

particles containing pLV-EF1A-hRLN2-EGFP or pLV-EF1A-EGFP, respectively), transduction was performed with a multiplicity of infection (MOI; the ratio of infectious virions to cells) of 2, for both cell lines, at a final volume of 0.5 ml per well using the same method described above. Cells were sorted on the BD influx system flow cytometer at 72 h post-transduction. The GFP⁺ cells from the cultured BM-MSCs-eRLX+GFP and BM-MSCs-eGFP, respectively were collected and cultured until 80% confluency was reached (after ~7–10-days), before they were used for assessment of cell proliferation, cell differentiation, measurement of RLX levels using the human relaxin-2 ELISA or passaged for expansion. For long-term storage, cells were trypsinized, pelleted and resuspended in a freezing medium containing 30% FBS, 1% penicillin/streptomycin, and 5% dimethylsulfoxide (DMSO; Sigma-Aldrich, St Louis, MO, USA), frozen at -1 °C/min until reaching -80 °C, before being stored in liquid nitrogen. To ensure the stable transduction of both lentiviral vectors in long-term culture, flow cytometry was performed on a LSR Fortessa flow cytometer after 2 passages of flow sorting (P6) to quantify % GFP⁺ cells within BM-MSCs-eRLX+GFP and BM-MSCs-eGFP populations again, which represented ~77.5% and ~86.7% of each cell population, respectively (Fig. 1B), confirming the long-term incorporation of the vector construct in BM-MSCs using the transduction method used.

RXFP1 staining of BM-MSCs-eRLX + GFP

RXFP1 expression on BM-MSCs-eGFP (as control transduced cells) and BM-MSCs-eRLX+GFP was determined by immunofluorescence staining. Briefly, 4×10^4 cells, respectively, were cultured on a 12 mm glass coverslip (pre-coated with 0.1% gelatin) in a 24-well plate. Following overnight incubation at 37 °C, cells were fixed in 4% PFA for 10 min at room temperature, washed in PBS for 5 min (3 times) and blocked for non-specific protein binding in 2% Bovine serum albumin (BSA) for 1 h at room temperature. The fixed cells were then washed again in PBS for 5 min (3 times) and incubated with a rabbit polyclonal RXFP1 antibody (A9227 [35]; 1:2000 dilution; Immunodiagnostik AG, Bensheim, Germany) in 2% BSA overnight at 4 °C, whilst the negative control was incubated only with 2% BSA. On the second day, the primary antibody was washed with PBS, before cells were incubated with goat anti-rabbit Alexa-fluor 555 secondary antibody (A21428; 1:500; Invitrogen, Scoresby, Victoria, Australia) in 2% BSA for 1 h at room temperature, before washed 3 times with PBS. Nuclear counterstaining was performed by adding ~10 μ l of VECTASHEILD@ Antifade Mounting Medium (With DAPI; H-1200, Vector Laboratories) prior to coverslipping. Immunoreactive RXFP1 (red staining) was visualised at $\times 200$

magnification using the Leica AF6000LX microscope, in association with the GFP⁺ cells (green) and DAPI (blue)-stained cells, and merged using ImageJ software.

Proliferation assay

To assess whether viral transduction of BM-MSCs affected cell viability and proliferative capacity, BM-MSCs were seeded into 96-well plates at 5×10^3 cells per well containing 100 μ l of culture media, or media supplemented with RLX at 1 ng/ml or 10 ng/ml (in triplicate), and cultured at 37 °C, for 3- or 7-days. Separate sets of triplicate wells were used to culture BM-MSCs-eRLX+GFP or BM-MSCs-eGFP under the same condition. After 3- and 7- days of culture, cell proliferation was determined using the CellTiter 96 AQueous One Solution Proliferation Assay (Promega, Fitchburg, WI, USA) according to the manufacturer's instructions.

Differentiation assay

To assess whether RLX-expressing BM-MSCs had the multipotency of naive BM-MSCs, the adipogenic, osteogenic and chondrogenic potential of BM-MSCs-eRLX+GFP were assessed using the Human Mesenchymal Stem Cell Functional Identification Kit (SC006; R&D Systems, Minneapolis, MN, USA) at passage 6 (P6), as per the manufacturer's instructions. Adipocytes, osteocytes and chondrocytes were identified via positive histological staining with Oil-red-O, Alizarin red and alcian blue, respectively; or via immunohistochemical staining for fatty acid binding protein 4 (FABP4), osteocalcin and aggrecan, respectively. Adipocytes and osteocytes that were subjected to histological and immunofluorescent staining were imaged at $\times 200$ magnification using an Olympus fluorescent microscope and CellSens Software (version 1.15; Olympus, Bartlett, TN, USA), whereas the chondrocytes pellets were imaged with a fluorescent microscope (Provis AX70; Olympus).

Migration assay

The migration capacity of naive BM-MSCs, in the absence of presence of RLX (10 ng/ml), as well as BM-MSCs-eRLX+GFP or BM-MSCs-eGFP was determined over a 24 h (hr) period. To perform the assay, 2×10^4 cells were suspended in 70 μ L growth media and seeded into 2 well-silicone in 35 mm dishes for wound healing assay (Ibidi Inc., Fitchburg, WI, USA) and incubated at 37 °C for 24 h to form a confluent cell layer. Artificial wounds within the dishes were then created at a gap distance of $500 \pm 100 \mu$ m [35]. The dishes were replenished with 2 mL of MSC growth media supplemented with various treatments of interest. The number of cells that migrated to close the wound was assessed by using light microscopy. Photomicrographs of the migrated cells were captured at

0-, 2-, 4-, 6-, 12- and 24-h post-treatment. The percentage of gap closure area was determined using ImageJ software (NIH, Bethesda, MD, USA). The slope of the linear phase was used to characterise the average wound closure rate and was expressed as a % of that measured from the migration capacity of naïve BM-MSC controls.

Secretion profile of BM-MSCs-eRLX + GFP compared to naïve BM-MSCs

To characterise the secretion profile BM-MSCs-eRLX + GFP, a human cytokine array was performed using a Proteome Profiler Human XL Cytokine Array Kit (ARY022B; R&D Systems), from the 7-day cell culture supernatant of BM-MSCs-eRLX + GFP and naïve BM-MSCs (from $n=4$ separate supernatant samples per cell type). Briefly, the nitrocellulose membranes (containing capture and control antibodies spotted in duplicate) were blocked for 1 h, before incubating with 400 μ L of cell culture supernates (from 0.5×10^6 cells of each type) overnight at 4 °C on a rocking platform shaker. The membrane was then incubated for 1 h with the detection antibody cocktail, washed and incubated with streptavidin-HRP. Finally, the Chemi Reagent mix was spread on the membrane to obtain an autoradiograph, and the duplicate dots were quantified by densitometry using a ChemiDoc MP imaging System (Bio-Rad; South Granville, New South Wales, Australia). The OD of each duplicate dot (representing one cytokine/chemokine; see mean \pm SEM OD of the cytokine/chemokine intensity detected in STable 1 [Supplementary File]) from BM-MSCs-eRLX + GFP was corrected for that of the reference levels for each membrane and expressed relative to the corresponding

values from naïve BM-MSCs (% change compared to that secreted by naïve BM-MSCs alone), which was expressed as 0 in each case. Only the % change from the detectable cytokines are presented in Fig. 2F.

Exosome extraction from BM-MSCs-eRLX + GFP

P6 BM-MSCs-eRLX + GFP were grown to approximately 80% confluency and starved in DMEM supplemented with 1% FBS and 1% penicillin/streptomycin for 72 h. Media was collected and clarified at 2000 g for 30 min, followed by 0.45 μ m filtration. Clarified media was ultracentrifuged (Sorvall WX 100 + Ultracentrifuge; Beckman Coulter Type 70.1 Ti fixed-angle rotor) at 100,000 g for 1 h at 4 °C (Beckman Coulter Australia, Mount Waverley, Victoria, Australia). The top 9 ml of each tube was discarded, the bottom 1 mL was pooled and spun again using the same parameters, and the rest (conditioned medium) was stored at -80 °C. Media was aspirated, and the sides of the tubes were washed thoroughly with 500 μ L of PBS. Particle size and yields were determined using the Zetaview[®] PMX-120 Nanoparticle Tracking Analyzer (NTA) (Laser=488 nm, Sensitivity=80 AU, Shutter Speed=100 s⁻¹, Frame Rate=30/s). Analysis was conducted on a 1:100 dilution of isolated exosome stock (Max Area = 1000px, Min Area = 10px, Max Brightness = 30). A flowchart depicting the process of exosome extraction and detailing the size of the exosomes extracted is shown in Figure S1 [Supplementary File]. The extracted exosomes were lysed with RIPA Buffer (#9806; 10x) containing proteinase inhibitor (#5872; 100x) and PMSF (#8553; 200x; all from Cell Signaling Technology; Danvers, MA, USA) for measurement of H2 RLX levels.

(See figure on next page.)

Fig. 2 Proliferation, migration and cytokine-secretion capacity of BM-MSCs-eRLX + GFP. **A** RXFP1 (red staining) was detected on the cell surface of BM-MSCs-eRLX + GFP; which was colocalised with DAPI-nuclear (blue) staining. A negative control image is also provided in which the cells shown were not stained with the primary RXFP1 antibody used. **B** Representative images show the trilineage differentiation ability of BM-MSCs-eRLX + GFP (as per their naïve/unmodified counterparts) to differentiate in vitro into adipocytes, osteocytes and chondrocytes, as confirmed with histological and immunohistochemical staining (for adipocytes using oil-red O and fatty acid binding protein 4 (FABP4) staining; osteocytes using alizarin red and osteocalcin staining; and chondrocytes using alcian blue and aggrecan staining) colocalized with DAPI-staining. Scale bar = 2 mm or 100 μ m as indicated. **C** The mean \pm SEM 3-day and 7-day proliferation capacity of BM-MSCs alone or treated with 1 ng/ml or 10 ng/ml RLX vs BM-MSCs-eRLX + GFP or BM-MSCs-eGFP, and **D** 24-h migration capacity of these cells (expressed relative to that of the untreated naïve BM-MSCs). * $p < 0.05$ vs the (unstimulated) BM-MSCs group; as determined using a one-way ANOVA and Tukey's *post-hoc* test. **E** The ELISA-determined levels of H2 RLX that were produced by naïve BM-MSCs ($n=4$) vs BM-MSCs-eRLX + GFP ($n=4$) that were cultured for 3- and 7-days in vitro are also shown. **F** Additionally, 30 cytokines that were measurably altered (up- or down-regulated; as determined by a human cytokine array with antibodies to 105 cytokines) in the cell supernatant of BM-MSCs-eRLX + GFP that were cultured for a 7-day period are shown, which were expressed as the % change relative to their naïve BM-MSCs counterparts. Data are presented from $n=4$ separate experiments, and cytokines that play a role in immunomodulation, angiogenesis (tissue repair) and ECM remodeling/cell proliferation are grouped and highlighted. Data points between 200 and 15,000 are not shown due to the break in the y-axis. Abbreviations: MCP, monocyte chemoattractant protein; IL, interleukin; VCAM-1, vascular adhesion molecule-1; MIF, macrophage migration inhibitory factor; VEGF, vascular endothelial growth factor; IGF1, insulin growth factor binding protein; uPAR, urokinase-type plasminogen activator receptor; PDGF-AA, platelet-derived growth factor containing two A subunits; BDNF, brain-derived neurotrophic factor; FGF, fibroblast growth factor; SDF, stromal cell-derived factor; GDF, growth differentiation factor; DKK1, Dickkopf Wnt signaling pathway inhibitor 1

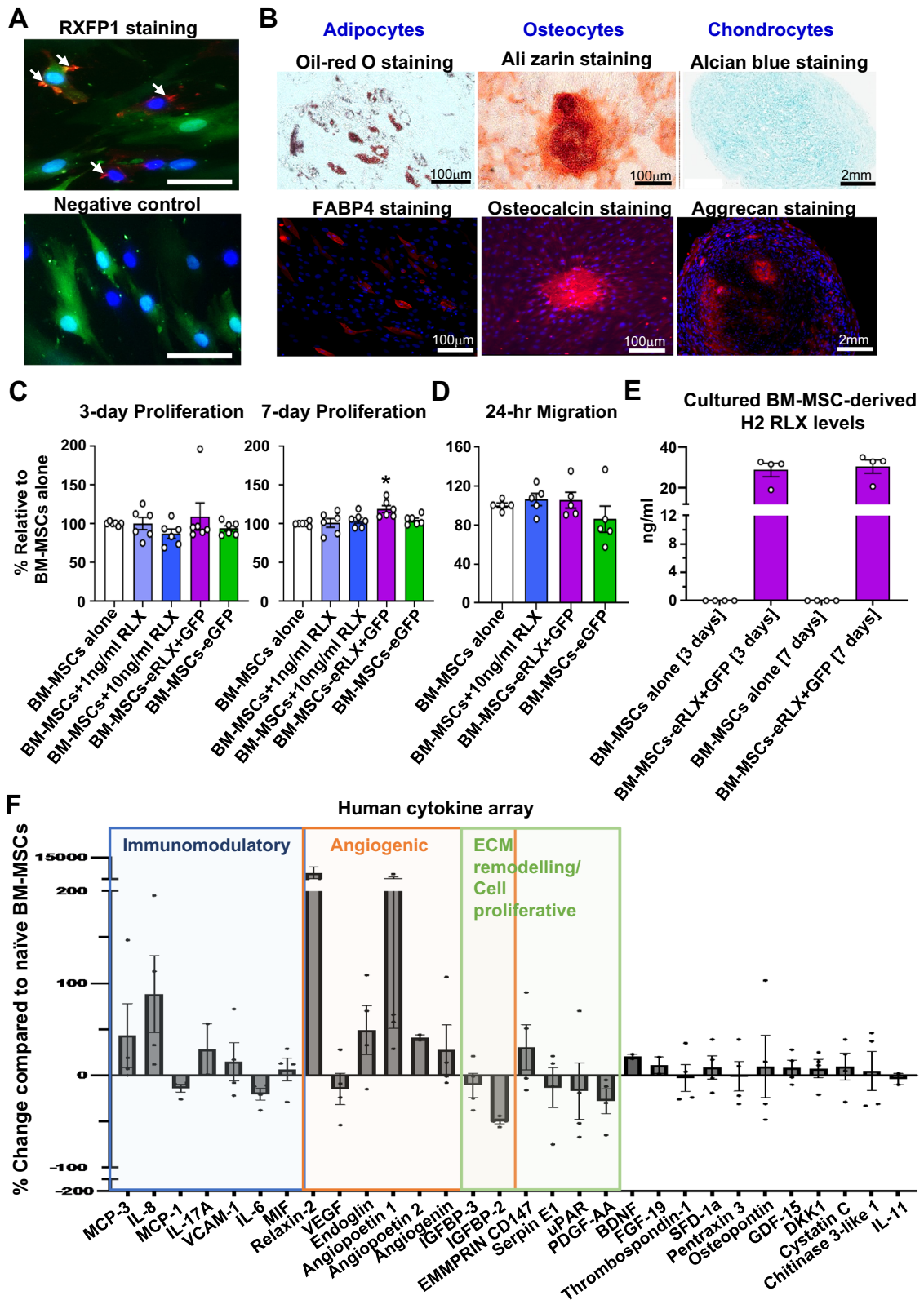


Fig. 2 (See legend on previous page.)

Animals

All animal care and experimental procedures performed adhered to the NIH guidelines for the Care and Use of Laboratory Animals for Scientific Purposes, and were approved by the Animal Ethics Committee of Monash University. The work has been reported in line with the ARRIVE guidelines 2.0. The sex of animals was considered in the study design: given that male mice are more prone to undergo a more rapid rate of kidney disease progression and hypertensive renal injury, in line with hypertension and CKD being more common in men compared to women [36], male mice were used since they provided a larger therapeutic window in which the efficacy of cell-based treatments evaluated could be measured. Initially, groups of equal size were designed using randomization and blinded analysis; although confounding variables were not controlled. 6-week-old male C57BL/6 J mice were obtained from Monash Animal Services (Monash University, Clayton, Victoria, Australia) to compare the renoprotective effects and biodistribution of BM-MSCs-eGFP versus BM-MSCs-eRLX + GFP in a model ischemia reperfusion injury (IRI; under animal ethics number: MARP/2022/29417). Mice subjected to IRI were anaesthetised with inhaled isoflurane (2–3% in oxygen; Baxter Healthcare) and provided analgesia (carprofen; s.c) just prior to surgery, and 24 h and 48 h post-surgery. 11–12-week-old male Balb/c mice were obtained from Monash Animal Services (under animal ethics number: MARP/2021/30019) to compare the therapeutic effects, biodistribution and safety of BM-MSCs-eGFP versus BM-MSCs-eRLX + GFP in a model of high salt (HS)-induced hypertensive nephropathy; which did not require any anaesthesia or analgesia. In the latter model, the therapeutic effects of BM-MSCs-eRLX + GFP were also compared to, or combined with, the current standard of care medication, perindopril. All mice were housed (in groups of four per cage) under a controlled environment, given a 5- to 6-day acclimatisation period, and maintained on a 12-h light/12-h dark cycle with free access to normal rodent lab chow (Barastock Stockfeeds, Pakenham, Victoria, Australia) and water.

In each case, power calculations were performed to ensure that adequate group sizes were used for the studies conducted; where it was determined that with a 20–25% standard deviation, we would be 80% powered to detect a 23–28% effect with $n=8$ animals per group. In either (the IRI or HS) model established, the effects of RLX alone was not assessed, since our previous work had already determined that the combined effects of RLX and BM-MSCs provide broader renoprotection over that of RLX alone in normotensive [29] and hypertensive [28] models of kidney disease.

Induction and treatment of a murine model of ischemia-reperfusion injury (IRI)

To assess the therapeutic effects of BM-MSCs-eRLX + GFP as a treatment for AKI, a unilateral IRI-induced model of AKI was established in 6-week-old male C57BL/6 J mice ($n=32$), weighing approximately 25–30 g. Mice were initially anaesthetised with 4% isoflurane in an induction chamber, and then maintained with 1–2% isoflurane via a nasal cone for the remainder of the surgery. Using a vascular clamp (0.4–1.0 mm; Fine Science Tools, Heidelberg, Germany), the renal pedicle (which included the renal artery and vein) was identified and clamped for 40 min. After 40 min, the clamp was removed and during this reperfusion stage, subgroups of mice were either i) left untreated (IRI group; $n=8$) or given an intra-renal injection of ii) 1×10^6 BM-MSCs-eGFP ($n=8$) or iii) 1×10^6 BM-MSCs-eRLX + GFP cells ($n=8$) (all suspended in 200 μ l PBS). iv) To compare the renoprotective effects of BM-MSCs-eRLX + GFP cells to that of BM-MSCs and RLX administered separately, a separate group of mice ($n=8$) had a small dorsal incision made during the ischemic period, in order to implant 7-day osmotic mini pumps (Model 1007D; with a release rate of 0.5 μ l/hour; ALZET, Cupertino, California, USA) containing RLX (Pump-RLX; 0.5 mg/kg/day). This dose of RLX had previously been found to produce circulating RLX levels of ~18–20 ng/ml in mice after 5-days [37]. During the reperfusion stage, these mice were injected with 1×10^6 BM-MSCs (suspended in 200 μ l PBS). v) A sham-operated control group ($n=8$) was also included with mice being anaesthetised and left flank incision made to expose the kidney, but the kidney remained untouched. The four groups of mice were maintained until 7-days post-sham or IRI surgery, before being killed for blood and kidney tissue collection and analysis.

Additionally, the in vivo tracking of transplanted BM-MSCs-eGFP and BM-MSCs-eRLX + GFP was conducted on a separate cohort of IRI mice ($n=24$), which were either subjected to IRI alone ($n=2$ per time point) or were subjected to IRI and received a single i.v.-injection of BM-MSCs-eGFP ($n=3$ per time point) or BM-MSCs-eRLX + GFP ($n=3$ per time point). As our previous work had determined that i.v.-administered BM-MSCs-eGFP immediately migrated to the lungs of IRI mice, but then homed to the injured kidney after 24 h and remained in the kidney after 72 h [34], IRI mice treated with BM-MSCs-eGFP or BM-MSCs-eRLX + GFP were then killed at 5-, 7- and 14-days post-transplantation for the analysis of the biodistribution of cells, and quantification of GFP⁺ cells within the kidney. At the appropriate time-points, mice were killed with an overdose of inhaled isoflurane (5% in oxygen) followed by cardiac puncture and

exsanguination, so that blood and appropriate organs could be isolated for analysis.

Induction and treatment of a murine model of high salt (HS)-induced hypertensive kidney disease

To assess the therapeutic effects of BM-MSCs-eRLX + GFP as a treatment for hypertensive CKD, a HS (2% NaCl in drinking water)-induced model of hypertension was established in 11–12-week-old male Balb/C mice ($n=40$; weighing 20–25 g) for 8-weeks; which was adapted from a previously published study [38]. Balb/c mice exhibited hypertension, kidney inflammation and fibrosis after 6-weeks of 2% NaCl drinking [38]. We therefore employed an 8-week model of HS loading, from which sub-groups of HS-fed mice were treated during the final two-weeks to assess the therapeutic impact of various treatments in mitigating the established salt-sensitive hypertension and related renal pathologies. The i) control group ($n=8$) was maintained on normal drinking water (NDW) for the 8-week period. At week-7 post-HS loading, subgroups of the $n=48$ HS-fed mice were randomised to either receive ii) no treatment (HS group; $n=8$); or an intravenous (i.v; tail vein) injection of iii) 1×10^6 BM-MSCs-eGFP (and then again on week-8 ($\times 2$); $n=8$); iv) BM-MSCs-eRLX + GFP ($\times 1$; $n=8$); v) BM-MSC-eRLX + GFP ($\times 2$; then again on week-8; $n=8$); vi) Pump-RLX delivered via an s.c. implanted 14-day osmotic minipump (0.5 mg/kg/day; Model 2002; with a release rate of 0.5 μ l/hour; ALZET) and i.v. injection of BM-MSCs (1×10^6 /mouse; and then again on week-8) (Pump-RLX + BM-MSCs; $n=8$); or vii) the angiotensin-converting enzyme inhibitor, perindopril (2 mg/kg/day via drinking water; a dose that induced anti-hypertensive effects without inducing weight loss [28, 39]; $n=8$) via drinking water.

In a separate study that assessed the renoprotective effects of BM-MSCs-eRLX + GFP ($\times 2$) in the presence of perindopril treatment, control groups of mice that were maintained on NDW ($n=8$) or HS ($n=24$; $n=8$ subjected to HS alone) for 8-weeks were again established. Additional sub-groups of HS-fed mice were then subjected to perindopril alone (as above; $n=8$); or perindopril + BM-MSCs-eRLX + GFP ($\times 2$; $n=8$). In both studies, all treatments were maintained for two-weeks, from weeks-7–8 post-HS, before all groups of mice were killed by an overdose of inhaled isoflurane (5% in oxygen) followed by cardiac puncture and exsanguination, for blood, heart and kidney tissue collection and analysis.

Safety study

To assess the long-term safety of BM-MSC-eRLX + GFP ($\times 2$) treatment, a further set of HS-fed ($n=9$) mice that were either untreated ($n=3$) or treated with

BM-MSC-eRLX + GFP ($\times 2$; $n=6$) were established and treated as outlined above; whilst NDW-fed mice ($n=3$) were also included as controls. All mice were maintained on NDW or HS drinking for 8-weeks (as above), but were then maintained on NDW for the further 9-months (39-weeks) after treatment cessation (to eliminate the long-term effects of HS-drinking as a confounding variable). At the completion of this period, when mice were 59-weeks of age, mice were transported to an independent Pathology company (Cerberus Sciences, Scoresby, Victoria, Australia) for histopathological assessment of various organs. The kidneys, adrenal glands, heart, aorta, lungs, thyroid gland, liver, spleen, stomach, pancreas, mesenteric lymph node, gall bladder, brain and skin of all mice were histologically assessed for abnormalities. Interstitial kidney fibrosis was also measured from the four groups of mice that survived the 9-month treatment cessation period; by Masson's trichrome staining of interstitial ECM deposition.

SBP measurements

Systolic blood pressure (SBP) measurements of all NDW and HS-fed mice were measured via tail cuff plethysmography, using the multichannel MC4000 Blood Pressure Analysis System (Hatteras Instrument Inc; Cary, NC, USA), at baseline and then fortnightly over the 8-week experimental period; and monthly over the 9-month treatment cessation period (for the safety study). At least 20 measurements per time point were pooled to obtain a mean value for each animal.

Confirmation of BM-MSC homing to the kidney

To determine if the i.v.-injected engineered cells could be detected in the kidneys and other organs of IRI or HS-fed mice, the left kidney pole, heart, lungs, spleen and liver of IRI mice; and left kidney pole and heart of HS-fed mice that were treated with BM-MSC-eGFP or BM-MSC-eRLX + GFP were subjected to genomic DNA (gDNA) extraction using a DNeasy Blood&Tissue kit (Qiagen, Clayton, Victoria, Australia) following the manufacturer's protocol. The extracted gDNA was then used for the analysis of *EGFP* gene expression by polymerase chain reaction (PCR). gDNA from 1×10^6 BM-MSCs-eGFP that were not injected into mice was used as a positive control. On the other hand, the replacement of gDNA with distilled water was included as a negative control. The PCR mixture contained the following components, including 10 μ L GoTaq Green Master Mix (Ref: M712B; Promega; Madison, WI, USA), 1 μ L forward primer: 5'-TAC GGC AAG CTG ACC CTG AAG TTC-3' and 1 μ L reverse primer: 5'CGT CGT CCT TGA AGA AGA TGG TGC G-3' primer pairs (Integrated DNA Technologies, Singapore), 1 μ L DNA template and 7 μ L of Nuclease-free

water. PCR mixtures were run under the following conditions: 94 °C for 2 min, 35 cycles (of denaturing for 30 s at 94 °C, annealing for 30 s at 60 °C, and extending for 1 min at 72 °C), then 72 °C for 7 min, before samples were held at 10 °C before collection. PCR products were then separated by electrophoresis on a 2% (w/v) agarose gel, where the primer sequences used were expected to produce a 196 base-pair product. Notably, 100 bp or 50 bp DNA ladders were used for gels containing DNA samples extracted from IRI or HS-fed mice, respectively. Gels were imaged with a ChemiDoc MP imaging System (Bio-Rad; South Granville, New South Wales, Australia).

Histology and immunohistochemistry

Serial paraffin-embedded left kidney Sects. (4 µm thickness; from the kidney mid-zone of IRI and HS-fed mice) were processed and stained with either haematoxylin and eosin (H&E) for the semi-quantification of inflammatory cell infiltration and proximal tubular damage [40]; picrosirius red-staining of interstitial collagen deposition [29, 41]; or Masson's trichrome staining of interstitial ECM deposition (for the safety study only) or glomerular matrix deposition (glomerulosclerosis) [28, 41], respectively. To visualize the localization of GFP⁺ cells in the kidneys from animals treated once-weekly with BM-MS-C-eGFP (×2) or BM-MS-C-eRLX+GFP (×2), separate left kidney frozen sections (from one kidney pole of these two groups) embedded in optimal cutting temperature (OCT) were sectioned into 6 µm thickness, fixed in 4% paraformaldehyde (PFA), and mounted with VECTASHEILD[®] Antifade Mounting Medium (with DAPI; H-1200, Vector Laboratories). Separate 6 µm frozen sections from the kidneys of NDW-fed mice (negative control) were also visualized. GFP⁺ cells within each section were imaged at ×400 magnification, using the DAPI filter for visualization of cell nuclei (blue staining), with a Leica AF6000LX microscope. To quantify the homing of the engineered cells, the number of GFP⁺ cells/field of view was determined in the kidneys of mice treated with once-weekly injections of BM-MS-C-eGFP (×2) or BM-MS-C-eRLX+GFP (×2), from 6 non-overlapping fields at ×200 magnification. Notably, the kidney samples were also stained with a goat anti-collagen IV polyclonal IgG (#1340-01; 100 dilution; SouthernBiotech, Birmingham, AL, USA) followed by a donkey anti-goat Alexa Fluor[™] 555 IgG (A21432; 1:500 dilution; Invitrogen) secondary antibody, to outline the basement membrane (red-staining) so that the location of GFP-labelled cells within the injured kidneys of mice could be determined.

Further serial paraffin sections obtained from the kidneys of IRI and HS-fed mice were also immunohistochemically (IHC) stained with either a rat monoclonal IgG2b antibody, Clone 222,414 (#MAB1817, 1:100

dilution; R&D Systems) to kidney injury molecule-1 (KIM-1; a marker of tubular epithelial injury), a rabbit polyclonal antibody (#ab5694, 1:1000 dilution; Abcam Antibodies, Cambridge, MA, USA) to α -smooth muscle actin (α -SMA; a marker of myofibroblast differentiation) or a rabbit polyclonal antibody (#ab28364, 1:150 dilution; Abcam Antibodies) to CD31 (an endothelial cell surface marker that was used to evaluate peritubular capillary density), followed by incubation with an anti-rat (#7077; 1:500 dilution; Cell Signaling Technology, Danvers, MA, USA) or anti-rabbit (#K4003; Agilent Technologies) secondary antibody, respectively. Additionally, the localization of pSmad2 in the kidney of HS-fed mice was semi-quantitated with immunofluorescent staining, using a rabbit monoclonal antibody to detect pSmad2 expression (#3108S), followed by exposure of sections to a goat polyclonal anti-rabbit Alexa Fluor[™] 594 IgG secondary antibody (1:500; Invitrogen). Furthermore, a rat monoclonal IgG2b antibody, clone CI:A3-1 was IF-stained to detect F4/80⁺ macrophage accumulation (#MCA497R, 1:100 dilution; Bio-Rad Laboratories, Portland, ME, USA), which was co-stained with a goat anti-collagen IV polyclonal IgG to visualize co-localization of F4/80⁺ macrophages with type IV collagen (to outline the kidney structure; #1340-01; 1:100 dilution; SouthernBiotech, Birmingham, AL, USA), followed by staining with goat anti-rat Alexa Fluor[™] 488 IgG (A11006; 1:500 dilution; Invitrogen) and donkey anti-goat Alexa Fluor[™] 555 IgG (A21432; 1:500 dilution; Invitrogen) secondary antibodies, respectively.

All slides subjected to histological, IHC or IF staining detailed above were scanned and captured with the Aperio Scanscope AT Turbo (Leica Microsystems Pty, Ltd, VIC, Australia) and assessed with Image J (FIJI) software (NIH, Bethesda, MD, USA). Morphometric analysis of each kidney section was randomly performed on 8–10 non-overlapping fields of view per section, at ×400 magnification by a blinded investigator. Total kidney inflammatory cell infiltration was semi-quantitated from H&E-stained kidney sections on a scale of 0–4 as previously described [40]. Tubulointerstitial fibrosis was determined from picrosirius red-stained kidney sections and was expressed as the % stained area per field analysed [29, 41]. To further assess glomerulosclerosis using Masson's trichrome-stained kidney sections, ~30 glomeruli were randomly selected from each section, with the severity of glomerulosclerosis scored based on a previously described method (from a scale of 0–4) [42]. All IHC- or IF-stained slides were semi-quantitated by the percentage of positive DAB (brown) staining or positive fluorescent (green) staining relative to the total area of the field analysed, respectively.

Flow cytometry

Flow cytometry was performed on cell suspensions from freshly isolated whole kidneys of NDW controls ($n=6$), HS-fed mice ($n=6$) and HS-fed mice treated once-weekly with BM-MS-C-eRLX + GFP ($\times 2$; $n=6$). Briefly, the right kidney of each mouse was digested mechanically using fine scissors, and then enzymatically by incubation for 30 min with 2 mL of kidney dissociation medium containing collagenase/dispase (3 mg/ml; 10,269,638,001; Roche), DNase type 1 (0.02%; 11,284,932,001; Roche) and CaCl₂ (0.05 mM) in sterile HANKS balanced salt solution. The digested tissue was passed through a 70 mm sterile filter (BD Biosciences, USA), before 10 ml of flow cytometry buffer (FACS buffer; PBS supplemented with 0.5% BSA and 5 mM EDTA) was added to stop the enzymatic reaction. Cells were pelleted by centrifugation at 400 g (at 4 °C) for 5 min and re-suspended in 2 ml RBC lysis buffer for 1 min at room temperature, before topping up with cold FACS buffer to 10 ml and centrifuging again for 5 min at 400 g. Finally, the cell pellet was resuspended in 2 ml of FACS buffer, in which 10 ul was subjected to cell counting. Samples were then centrifuged at 400 g for 4 min and stained with the fluorochrome-conjugated antibody cocktail (listed in STable 2 [Supplementary File]) for 20 min at 4 °C in the dark. FcR blocking reagent (1:100 dilution, Miltenyi Biotec, Bergisch Gladbach, Germany) was used to exclude any non-specific binding of antibodies to cells expressing the Fc receptor. The stained cells were centrifuged at 400 g for 4 min, and washed and resuspended in FACS buffer with PI (1:500). All samples were analysed using Fortessa X20 instrument controlled by FlowDiva software (BD Biosciences, Melbourne, Victoria, Australia). Data were analysed using FlowJo software (see Figure S2 [Supplementary File] for the gating strategy used).

Enzyme-linked immunosorbent assay (ELISA)

The H2 RLX-specific Quantikine ELISA (DRL200; R&D systems, Minneapolis, MN, USA) was used to assess RLX levels in the supernatants of 1×10^6 BM-MS-C-eRLX + GFP cultured for 3- or 7-days; from the conditioned medium and $1-1.25 \times 10^9$ lysed exosomes collected from BM-MS-C-eRLX + GFP; and from the circulation of IRI- or HS-fed that were treated with BM-MS-C-eGFP or BM-MS-C-eRLX + GFP.

Total protein was also extracted from an injured kidney pole of IRI and HS-fed mice, using a previously described method [43]. Mouse DuoSet ELISA kits (R&D Systems) were used to assess the expression of the pro-inflammatory markers: monocyte chemoattractant protein (MCP)-1 (DY479-05), tumour necrosis factor (TNF)- α (DY410-05) and interleukin (IL)-1 β (DY401-05) from

HS-fed mice; and the pro-fibrotic marker: transforming growth factor (TGF)- β 1 (DY1679-05) in both in vivo models established. In all cases, duplicate aliquots per sample were assessed by ELISA analysis in accordance with the manufacturer's instructions. All endpoints were expressed as ng/ml.

Gelatin zymography

The same tissue extracts (used for ELISA analysis) from HS-hypertensive mice were separately used to assess the activity of MMP-2 (gelatinase A) and MMP-9 (gelatinase B) by gelatin zymography. Briefly, equal amounts of kidney extracts containing 10 μ g of protein per sample were loaded on 7.5% acrylamide gels containing 1 mg/ml gelatin as described previously [28, 43]. Gelatinolytic activity of glycosylated (G), latent (L) and active (A) MMP-2 or -9 was each visualized as clear bands and the optical density (OD; in arbitrary units) of each A-band was quantified by densitometry using a GS710 Calibrated imaging Densitometer (Bio-Rad Laboratories, Gladesville, New South Wales, Australia). The mean \pm SEM OD A-MMP-2 or A-MMP-9 was then measured and expressed as a fold-change of the mean value obtained from the NDW control group (which was expressed as 1).

Assessment of kidney function

At 8-weeks post-HS loading, all mice were individually housed in metabolic cages for 24-h (hr) urine collection. The urinary protein level (as a measure of proteinuria) was determined for each sample using the Bradford protein assay (Bio-Rad Protein Assay Dye Reagent Concentration; Gladesville, NSW, Australia) [41]. Urinary and plasma creatinine concentrations were measured using Creatinine assay kits (ab65340; Abcam, Cambridge, UK) according to the manufacturer's instructions, and were used to derive creatinine clearance using the following formula described previously [41]:

$$\text{Creatinine clearance (mL/24hr)} = \frac{\text{Urine creatinine concentration (nmol/mL)} \times \text{urine volume (mL/24hr)}}{\text{Plasma creatinine concentration (nmol/mL)}}$$

Statistical analysis

Data were expressed as the mean \pm SEM unless otherwise stated and were statistically analysed using GraphPad Prism (v9.3.0; GraphPad Software Inc, San Diego, CA, USA). SBP was analysed with a two-way analysis of variance (ANOVA; treatment \times time), while all the other data were analysed with a one-way ANOVA. Post hoc tests were only conducted if the overall ANOVA p-value achieved statistical significance (i.e., $p < 0.05$) and there was no significant variance in homogeneity. A Tukey's post-hoc test was conducted to allow for multiple comparisons between groups. Non-parametric (Kruskal-Wallis) tests were conducted for data that were graded

based on a scoring system (i.e. inflammation score, tubular abnormalities, protein cast formation, glomerulosclerosis); or normalised to the control group (i.e. Relative OD A-MMP-2 and A-MMP-9). All data were included unless any values were >2 standard deviations (SDs) from the mean. In the case of A-MMP-2 and A-MMP-9 levels, $n=6$ samples per group were analysed. Differences were considered statistically significant at $p<0.05$, and the threshold value was not varied during the study.

Results

Generation and characterisation of engineered BM-MSCs

Human BM-MSCs were transduced with a lentivirus containing human relaxin-2 cDNA (RLX) and green fluorescent protein (GFP), under a eukaryotic translation elongation factor-1 α promoter (termed BM-MSCs-eRLX+GFP; Fig. 1A) or GFP alone (BM-MSCs-eGFP). These BM-MSCs-eRLX+GFP and BM-MSCs-eGFP were characterised to confirm their cellular identity using the minimum criteria established by the International Society for Cellular Therapy [44]. Flow cytometry revealed transduction efficiencies of 72.4% and 94.4% at a multiplicity of infection of 2, for passage 4 (P4) BM-MSCs-eRLX+GFP and BM-MSCs-eGFP, respectively, from which both showed spindled-shaped morphology and expression of GFP (in 77.5% and 86.7% of P6 BM-MSCs-eRLX+GFP and BM-MSCs-eGFP, respectively; Fig. 1B). BM-MSCs-eRLX+GFP expressed RXFP1 (Fig. 2A) on their cell surface and were able to functionally differentiate into adipocytes, osteocytes and chondrocytes as evidenced by positive histological staining with Oil-red-O, Alizarin red and alcian blue, respectively; or immunohistochemical staining for fatty acid binding protein 4 (FABP4), osteocalcin and aggrecan, respectively (Fig. 2B).

Compared to the proliferation and migration capacity of 1×10^6 naïve BM-MSCs in culture, 1×10^6 BM-MSCs stimulated with either 1 ng/ml or 10 ng/ml RLX, or 1×10^6 BM-MSCs-eRLX+GFP or BM-MSC-eGFP did not undergo any further proliferation after 3-days (Fig. 2C) or migration after 24-h (Fig. 2D). However, 1×10^6 BM-MSCs-eRLX+GFP did undergo significantly increased proliferation (by ~18%) after 7-days (Fig. 2C), and produced 29 ± 3 ng/ml and 31 ± 3 ng/ml RLX in the supernatant after 3- and 7-days of culture, respectively (Fig. 2E). These RLX levels had previously been shown to attenuate TGF- β 1-induced human myofibroblast-induced collagen production and promote myofibroblast-mediated collagenase activity in vitro [45–47]. Detectable levels of RLX were also measured from the exosomes that were isolated and lysed from BM-MSCs-eRLX+GFP (Figure S1 [Supplementary File]) that were cultured for 3-days (~181.4 pg/ml), whereas the conditioned media from the exosome extraction contained ~2.3 ng/ml of

RLX. This suggested that the RLX secreted from BM-MSCs-eRLX+GFP was predominantly secreted by the cells as a soluble peptide rather than being packaged within BM-MSC-derived exosomes.

Protein secretion profile of BM-MSCs-eRLX + GFP

After 7-days of culture, BM-MSCs-eRLX+GFP secreted an enhanced but finely tuned immunomodulatory, angiogenic and ECM-remodelling/cell proliferative capacity compared to naïve BM-MSCs (Fig. 2F). The increased secretion of monocyte chemoattractant protein (MCP)-3 (by ~43%) and interleukin (IL)-8 (by ~88%) by BM-MSCs-eRLX+GFP may have been linked to the immunomodulatory effects of these cells in regulating macrophage and neutrophil trafficking, respectively. In a complementary manner, BM-MSCs-eRLX+GFP released lower levels of MCP-1 (by ~14%) and IL-6 (by ~21%) compared to naïve BM-MSCs, which may have been related to their anti-inflammatory effects. Regarding ECM remodelling, BM-MSCs-eRLX+GFP secreted less pro-fibrotic mediators such as insulin-like growth factor binding protein (IGFBP)-2 (by ~50%), IGFBP-3 (by ~11%), serpin E1, urokinase-type plasminogen activation receptor (uPAR) and platelet-derived growth factor containing two A subunits (PDGF-AA) (by ~13–28%), coupled with higher levels of CD147 (inducer of MMPs; by ~31%). Furthermore, BM-MSCs-eRLX+GFP showed heightened secretion of tissue-reparative factors including angiopoietin-1 (by ~tenfold), endoglin (by ~49%) and angiogenin (by ~28%), and produced a significantly higher amount of RLX compared to naïve BM-MSCs. Importantly, several tumorigenic-related factors were down-regulated by BM-MSCs-eRLX+GFP, such as IGFBP2, vascular endothelial growth factor (VEGF) and uPAR, compared to that released by naïve BM-MSCs, which pointed to the potential safety of utilising the therapeutic impact of these cells.

BM-MSCs-eRLX + GFP homed to the kidneys of IRI and HS-fed mice

EGFP gene expression (expected size 196 bp) was identified by PCR analysis in the kidneys of IRI mice, 5-, 7- and 14-days after a single i.v.-injection of BM-MSCs-eRLX+GFP (Fig. 3A-C); and in HS-fed mice, 7-days after a once-weekly i.v. injection of BM-MSCs-eRLX+GFP ($\times 2$), or 14-days after a single i.v.-injection of BM-MSCs-eRLX+GFP ($\times 1$), at 8-weeks post-HS loading (Fig. 3D-F). The EGFP expression identified in the kidneys of these animals corresponded to the same product that was derived from 1×10^6 BM-MSC-eGFPs that were not injected into mice (positive control). EGFP gene expression was also identified in other organs of IRI mice such as the lungs, heart, spleen and liver 5–14-days after a

single injection of cells (potentially owing to the transportation of cells to these organs during the reperfusion phase in which there is an increase in blood flow; Fig. 3A), but was not identified in the heart of HS-fed mice (Fig. 3D). No *EGFP* expression, however, was detected in the kidneys of sham or normal drinking water (NDW)-fed controls or when distilled water replaced cDNA (as negative controls). Furthermore, GFP-labelled cells were detected by fluorescence microscopy and predominantly localised to DAPI-nuclear stained cells within the renal tubular regions of IRI mice that were injected once with BM-MSCs-eGFP or BM-MSCs-eRLX + GFP (Fig. 3B) or HS-fed mice that were injected once-weekly with BM-MSCs-eGFP or BM-MSCs-eRLX + GFP (Fig. 3E), but not NDW-fed mice (negative control). Quantitative analysis of these GFP-labelled cells revealed a trend towards an increase in the number of GFP⁺ cells that had infiltrated the kidney of IRI + BM-MSC-eRLX + GFP-treated mice after 5-days (by ~87%) and 7-days (by ~54%) post-administration (Fig. 3C), compared to their BM-MSC-eGFP-treated counterparts. Similarly, ~74% more GFP⁺ cells were detected in the kidneys of HS + BM-MSCs-eRLX + GFP (×2)-treated mice compared to their BM-MSCs-eGFP (×2)-treated counterparts ($p=0.08$ vs the BM-MSCs-eGFP-treated group; Fig. 3F).

Additionally, circulating RLX levels were detected in IRI mice treated with BM-MSCs-eRLX + GFP (0.07 ± 0.05 ng/ml; Fig. 3G) by 7-days post-cell administration. Comparatively, plasma RLX levels were slightly higher in HS + BM-MSCs-eRLX + GFP-treated mice, 14-days after a single i.v.-injection of cells (0.4 ± 0.1 ng/ml) or 7-days after the second injection of cells (1.7 ± 0.2 ng/ml), which mirrored circulating RLX levels found in pregnant women [48] and in human subjects enrolled in various clinical trials who received 25–100 µg/kg/day of RLX [49].

BM-MSCs-eRLX + GFP attenuated IRI-induced kidney damage and fibrosis

Compared to sham-operated controls, IRI mice maintained similar body weight (BW), kidney weight (KW) and KW:BW ratio (STable 3 [Supplementary File]), but underwent a significant increase in kidney inflammation, structural damage (by 5–6.5-fold; Fig. 4A and F) and KIM-1-associated tubular damage (by 10.6-fold; Fig. 4B and G) by 7-days post-injury. Whilst each of these elevated measures were unaffected by BM-MSCs-eGFP treatment alone, BM-MSCs-eRLX + GFP treatment attenuated the IRI-induced increase in kidney inflammation and structural damage (by ~50–55%; Fig. 4F) and significantly prevented the KIM-1-stained tubular damage (Fig. 4G), to levels that were not different to that measured in sham controls. In each case, this was to an equivalent extent as Pump-RLX + BM-MSC treatment administered separately.

IRI mice also presented with significantly increased interstitial kidney fibrosis (by 2.1-fold; Fig. 4C and H), glomerulosclerosis (by one-fold; Fig. 4D and I), interstitial myofibroblast accumulation (by 4.5-fold; Fig. 4E and J) and TGF-β1 levels (by 0.6-fold; Fig. 4K) at 7-day post-injury, compared to that measured in sham controls. BM-MSCs-eGFP treatment only effectively suppressed the IRI-induced interstitial kidney fibrosis (Fig. 4H) and TGF-β1 levels (Fig. 4K) after 7-days of treatment, but did not affect the other measures of fibrosis evaluated. In comparison, BM-MSCs-eRLX + GFP treatment equivalently prevented these measures in addition to the IRI-induced glomerulosclerosis (Fig. 4I), and also attenuated the IRI-induced interstitial myofibroblast accumulation (by 33%; Fig. 4J), to levels that were not different to that measured in sham-operated controls. In each case, this was to an equivalent extent as Pump-RLX + BM-MSC treatment administered separately. These findings

(See figure on next page.)

Fig. 3 Confirmation that i.v.-injected BM-MSCs-eRLX + GFP homed to the injured kidney of IRI and HS-fed mice post-transplantation. **A** Shown are representative images of SYBR Safe-stained 1.5% agarose gels that indicate a PCR product corresponding to *EGFP* (at the expected size of 196 bp) from either 1×10^5 cultured BM-MSCs-eGFP that were not injected into mice (positive (+ve) control) or the kidneys, hearts, lungs, livers and spleens of IRI mice at 5-days, 7-days and 14-days post-a single injection of BM-MSCs-eGFP or BM-MSCs-eRLX + GFP; or **D** from the kidney and heart of HS fed-mice 7-days after the second injection of BM-MSCs-eGFP (×2) or BM-MSCs-eRLX + GFP (×2) that were once-weekly injected at weeks-7 and -8 post-HS feeding or 14-days after a single-i.v.-injection of BM-MSCs-eRLX + GFP (×1) that was administered at the beginning of week-7 post-HS feeding. The full-length blots of panel **A** and **D** are shown in Supplementary Fig. 4 and Supplementary Fig. 5, respectively. **A, D** This PCR product was not found in the negative (-ve) control reaction, in which distilled water (dH₂O) replaced cDNA, or from the genomic DNA extracted from **A** these organs of IRI mice that were not injected with any cells; or **D** from the DNA extracted from the kidneys or heart of NDW-fed control mice. In each case, a **A** 100 bp or **D** 50 bp DNA ladder was included. **B, E** GFP-labelled cells (indicated by the white arrows) were also detected by fluorescence microscopy and were predominantly co-localised with DAPI-stained cells within the tubules of the left kidney of **B** IRI mice or **E** HS-fed mice that were injected with BM-MSCs-eGFP or BM-MSCs-eRLX + GFP, but not in **B** untreated IRI control or **E** NDW-fed control mice. The basement membrane structure (collagen IV) was outlined by red fluorescence. **C, F** Also shown is the mean ± SEM of the quantification of GFP⁺ cells/field from 6 non-overlapping fields each sample at ×200 magnification; from **(C)** $n=2-3$ mice per time-point per group from the IRI model; and **F** $n=6$ mice per group from the HS model. Scale bar = 100 µm in each case. **G** Additionally shown is the mean ± SEM plasma H2 RLX levels from each group shown; from $n=6$ mice per group

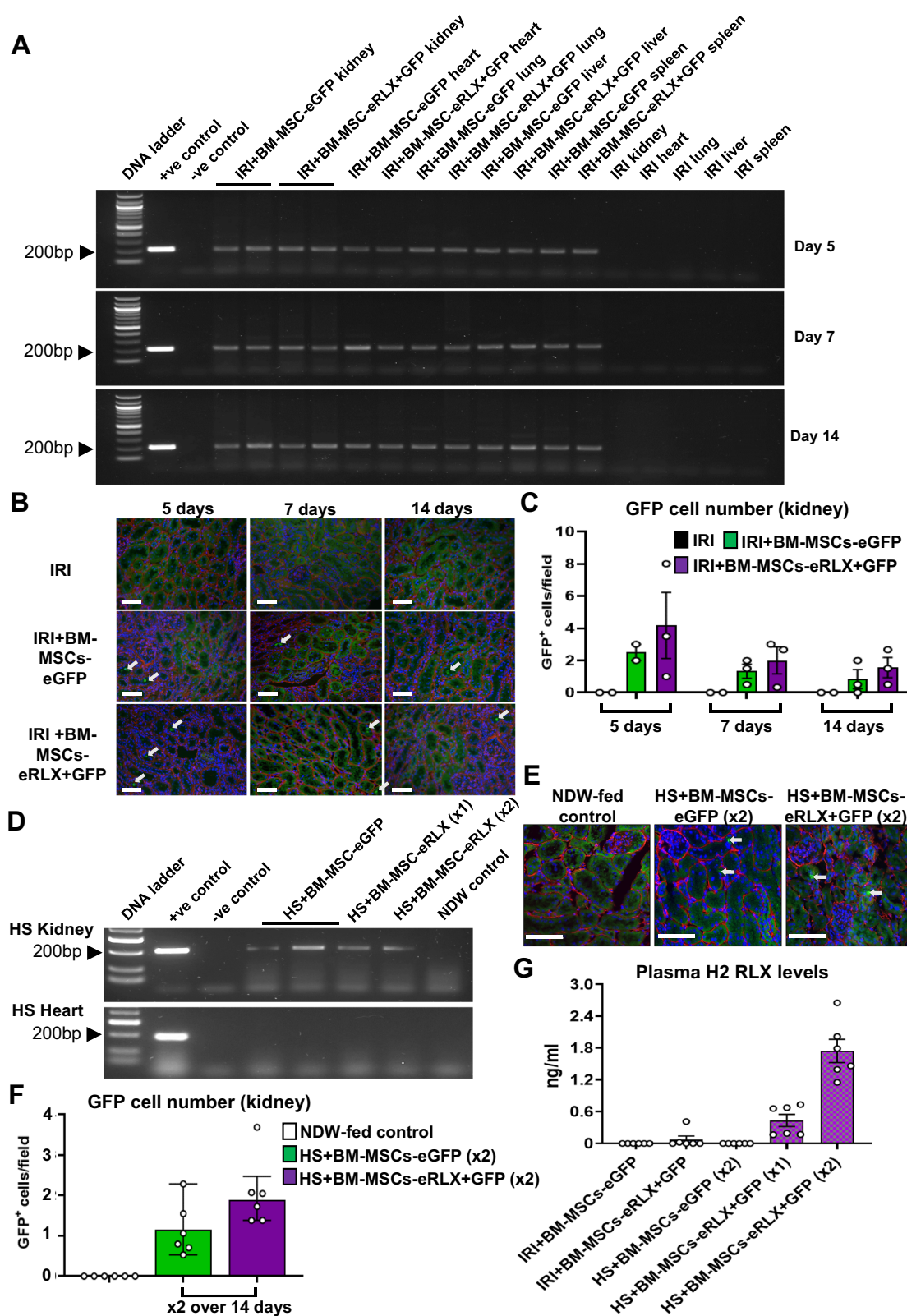


Fig. 3 (See legend on previous page.)

demonstrated the broader renoprotection offered by BM-MSCs-eRLX + GFP over BM-MSCs-eGFP against IRI.

BM-MSCs-eRLX + GFP therapeutically reduced HS-induced hypertension and renal vascular rarefaction

Compared to normal drinking water (NDW)-fed mice, HS (2% NaCl)-fed mice underwent a 10–15% loss of BW, in the absence of any marked changes in KW or KW:BW ratio (STable 3 [Supplementary File]), and a progressive increase in SBP, which reached ~20 mmHg above baseline measurements after 8-weeks (Fig. 5A). All treatments blunted the HS-induced loss of BW when administered from weeks 7–8, towards that of NDW-fed mice. Furthermore, when administered once-weekly from weeks 7–8 ($\times 2$), BM-MSCs-eGFP blunted (by 11–12 mmHg), whilst BM-MSCs-eRLX + GFP or Pump-RLX + BM-MSCs significantly normalised the HS-induced increase in SBP, to the same extent as perindopril treatment (Fig. 5A). In line with an elevated BP triggering renal vascular endothelial damage and dysfunction [50], HS-fed mice had significantly reduced kidney expression of CD31⁺ peritubular capillary density after 8-weeks (by ~35–40%; Fig. 5B and H) compared to their NDW-fed controls. Consistent with the treatment-effects on SBP, the HS-induced loss of perivascular capillary density was unaffected by BM-MSCs-eGFP ($\times 2$) treatment, but was restored to levels measured in NDW-fed mice by BM-MSCs-eRLX + GFP ($\times 2$), Pump-RLX + BM-MSCs or perindopril treatment (Fig. 5B and H).

BM-MSCs-eRLX + GFP therapeutically reduced the HS-induced kidney inflammation, tubular damage and fibrosis

Compared to NDW-fed controls, HS-fed mice exhibited interstitial matrix expansion and significantly increased kidney inflammation (Fig. 5C and I), which consisted of F4/80⁺ macrophage (by 7–8-fold; Fig. 5D and J), CD45⁺F4/80⁺CD206⁻ M1-like macrophage,

CD45⁺F4/80⁺CD206⁺ M2-like macrophage and CD45⁺CD11⁺ dendritic cell (Figure S2 [Supplementary File]) infiltration. HS-fed mice also presented with tubular KIM-1-associated damage (by 8.7-fold; Fig. 5E and K); pro-inflammatory monocyte chemoattractant protein-1 (MCP-1; by 1.6-fold), tumour necrosis factor (TNF)- α (by 1.8-fold) and interleukin (IL)-1 β (by ten-fold) (Figure S3 [Supplementary File]) levels; interstitial kidney fibrosis (by 3.7-fold; Fig. 5F and L); glomerular matrix accumulation (by 0.5-fold; Fig. 5G and M); interstitial myofibroblast accumulation (by 1.9-fold; Fig. 6A and D); kidney TGF- β 1 expression (by 1.8-fold; Fig. 6E); phosphorylated Smad2 (pSmad2) expression (by eight-fold; Fig. 6B and F); and matrix metalloproteinase (MMP)-2 activity (by 2.9-fold; Fig. 6C and H) after 8-weeks.

BM-MSC-eGFP ($\times 2$) treatment significantly reduced the HS-induced TNF- α levels (Figure S3 [Supplementary File]), interstitial kidney fibrosis (Fig. 5L), TGF- β 1 (Fig. 6E) and pSmad2 (Fig. 6F) levels, attenuated the HS-induced glomerulosclerosis to levels that were not different to that measured in NDW-fed controls (Fig. 5M), and increased MMP-2 activity (Fig. 6C and H) after 2-weeks of treatment. However, these cells failed to affect the HS-induced kidney inflammation (Fig. 5I) including macrophage infiltration (Fig. 5J), KIM-1-associated tubular damage (Fig. 5K), interstitial myofibroblast accumulation (Fig. 6D) or MMP-9 activity (Fig. 6C and G). On the other hand, all these inflammatory measures including M1-like macrophage infiltration, dendritic cell infiltration (Figure S2 [Supplementary File]), kidney MCP-1 and TNF- α levels (Figure S3 [Supplementary File]), as well as measures of fibrosis were significantly reduced or attenuated by BM-MSC-eRLX + GFP treatment. In each case, this was to an equivalent extent as Pump-RLX + BM-MSC treatment administered separately. However, only BM-MSC-eRLX + GFP treatment also significantly

(See figure on next page.)

Fig. 4 The effects of IRI and the treatments evaluated on kidney inflammation, tubular damage and fibrosis. **A, B** Representative images of **A** H&E-stained and **B** KIM-1 immunohistochemically stained kidney sections (taken at $\times 400$ magnification) show the extent of **A** kidney structural changes, protein cast formation (arrow), tubular dilation (*) as well as inflammatory cell aggregates (#); and **B** KIM-1 (brown staining)-associated tubular epithelial damage, respectively, in each group studied. **C–E** Representative images of **C** picrosirius red-stained, **D** Masson's trichrome-stained and **E** α -SMA immunohistochemically-stained kidney sections (at $\times 400$ magnification) show the extent of **C** red-stained tubulointerstitial and **D** blue-stained glomerular matrix deposition, as well as **E** brown-stained interstitial myofibroblast accumulation in each of the groups evaluated, respectively; from $n = 7–8$ mice per group. Scale bar = 100 μ m in each case. **F–K** Also shown is the semi-quantification of the **F** median \pm IQR inflammatory cell infiltration within the kidney; or the mean \pm SEM (**G**) KIM-1 staining per field analysed; **H** % interstitial kidney fibrosis staining per field analysed; **J** % α -SMA staining per field analysed; or **K** TGF- β 1 expression levels (determined by ELISA analysis of kidney protein extracts), as well as the **I** median \pm IQR glomerulosclerosis score; from $n = 8$ non-overlapping fields of view or 30 glomeruli per section analysed; from $n = 7–8$ mice per group. * $p < 0.05$, ** $p < 0.01$, *** $p < 0.001$ vs the sham-operated group; # $p < 0.05$, ## $p < 0.01$ vs the IRI alone group; + $p < 0.05$ vs the IRI + BM-MSC-eGFP group; as determined using **G, H, J, K** a one-way ANOVA and Tukey's *post-hoc* test or **F, I** a non-parametric Kruskal–Wallis test with Dunn's *post-hoc* analysis

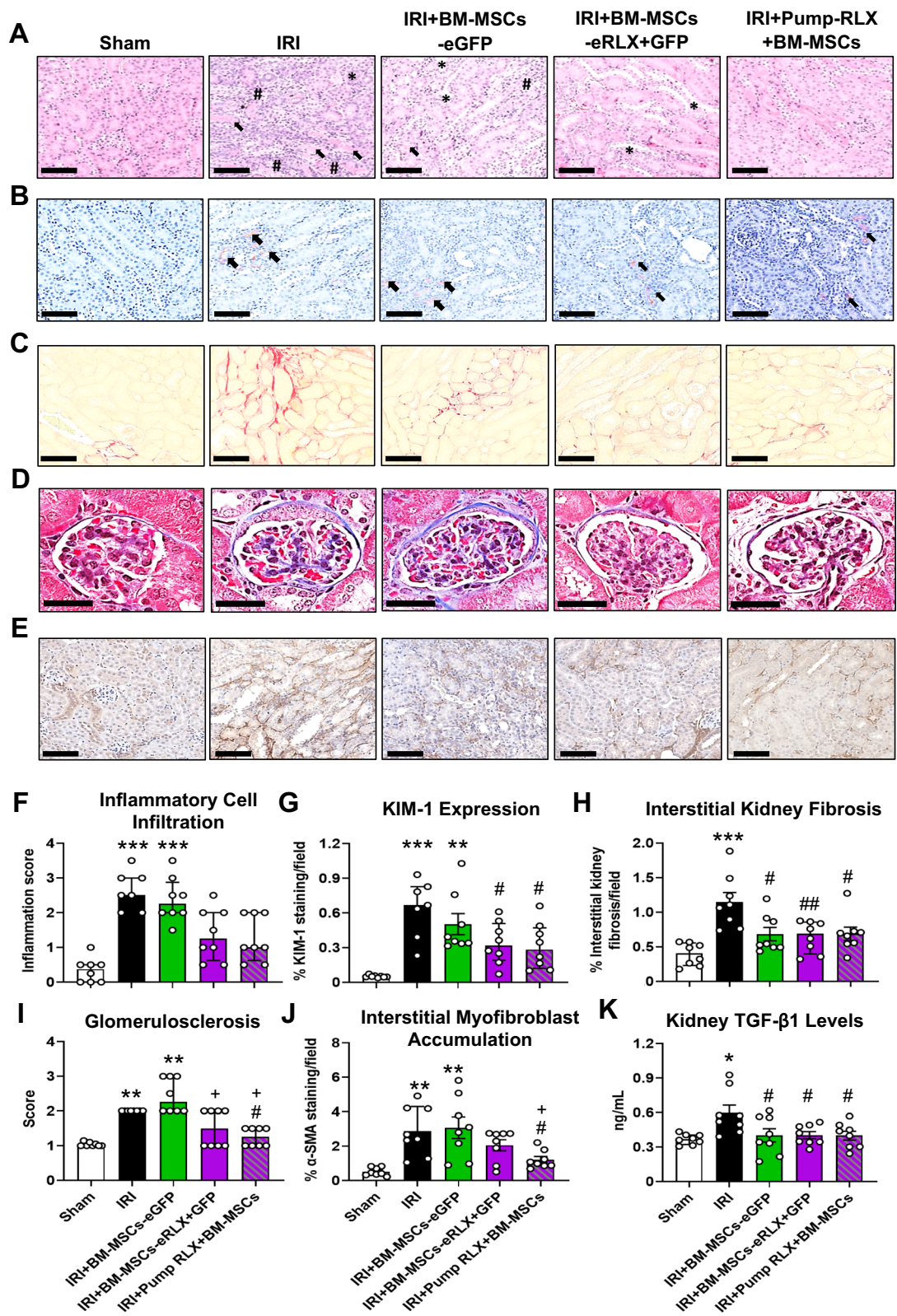


Fig. 4 (See legend on previous page.)

promoted both collagen-degrading MMP-9 (Fig. 6G) and MMP-2 (Fig. 6H) activity in HS-fed mice.

Notably, i) a single injection of BM-MSCs-eRLX + GFP ($\times 1$) ameliorated the HS-induced KIM-1-associated tubular damage, TNF- α , interstitial fibrosis, glomerulosclerosis and pSmad2 levels, and significantly promoted MMP-9 and MMP-2 activity to an equivalent extent as once-weekly administration of BM-MSCs-eRLX + GFP ($\times 2$), 14-days after being injected; and ii) all BM-MSC-based therapies reduced the HS-induced interstitial kidney fibrosis to a greater extent than perindopril (Fig. 5L). This was likely due to the greater ability of all BM-MSC-based therapies to promote gelatinase activity (Fig. 6G and H) compared to perindopril.

BM-MSCs-eRLX + GFP therapeutically restored the HS-induced kidney functional impairment

HS-fed mice exhibited significantly increased proteinuria (by one-fold; Fig. 6I) but reduced creatinine clearance (by 0.5-fold; Fig. 6J) after 8-weeks. Both measures of kidney impairment were only significantly ameliorated by BM-MSCs-eRLX + GFP or Pump-RLX + BM-MSC treatment, but not by BM-MSCs-eGFP nor perindopril treatment. Once again, these collective findings demonstrated the broader renoprotection offered by BM-MSCs-eRLX + GFP over BM-MSCs-eGFP or ACE inhibition against HS-induced nephropathy.

BM-MSCs-eRLX + GFP maintained their broad therapeutic efficacy in the presence of ACE inhibition

It was also determined if BM-MSC-eRLX + GFP could maintain their therapeutic efficacy (as an adjunct therapy) in the presence of a frontline treatment for CKD (such as perindopril), when administered to a separate cohort of HS-fed mice. In line with the findings presented in Fig. 5 and Fig. 6, perindopril treatment abrogated the HS-induced increase in SBP (Fig. 7A) and proteinuria (Fig. 7J), and partially reduced interstitial kidney fibrosis

(by $\sim 30\%$; Fig. 7C and G) and myofibroblast accumulation (by $\sim 45\%$; Fig. 7E and I) after 2-weeks, but failed to affect the HS-induced kidney inflammation (Fig. 7B and F), glomerulosclerosis (Fig. 7D and H) or the loss of creatine clearance (Fig. 7K). Comparatively, perindopril and BM-MSCs-eRLX + GFP treatment of HS-fed mice normalised the HS-induced increase in SBP to an equivalent extent as perindopril treatment alone, but significantly reduced all measures of kidney inflammation, fibrosis and function evaluated to levels measured in NDW-fed mice. Notably, the combined effects of perindopril and BM-MSCs-eRLX + GFP reduced the HS-induced interstitial kidney fibrosis (Fig. 7G) and restored the impairment of creatine clearance (Fig. 7K) to a significantly greater extent than perindopril treatment alone; confirming that BM-MSCs-eRLX + GFP could maintain their broad renoprotective effects in the presence of ACE inhibition.

Evaluation of the long-term safety and anti-fibrotic efficacy of BM-MSCs-eRLX + GFP

As the FDA requires that the safety of any cell-based therapy is assessed 6-to-9 months after treatment cessation, the long-term safety and renal anti-fibrotic efficacy of BM-MSCs-eRLX + GFP was assessed in HS-fed mice 9-months after treatment cessation. HS-fed mice exhibited a gradual elevation in SBP (Fig. 8A), reaching ~ 25 – 30 mmHg above baseline measurements taken after 6–12-weeks. These hypertensive mice had interstitial kidney fibrosis levels (0.9–2.4% per field; Fig. 7B and C) that had moderately resolved compared to what was measured at 8 weeks post-HS consumption (Fig. 5L), but were still significantly higher than that measured in their NDW-fed counterparts (0.4–0.6% per field). Notably, this HS-induced rise in SBP partially resolved (by ~ 15 – 20 mmHg) by 16–47-weeks post-HS discontinuation, but remained at ~ 15 – 20 mmHg above respective measurements taken at baseline during this interval. The HS-induced increase in SBP was significantly reduced by

(See figure on next page.)

Fig. 5 The effects of HS and the treatments evaluated on systolic blood pressure (SBP), kidney endothelial and tubular epithelial damage, kidney inflammation and fibrosis. **A** Shown is the mean \pm SEM SBP, from week-0 to week-8 of the HS-induced model established and treated; from $n = 8$ mice per group. **B–G** Representative images of **B** CD31⁺ immunostaining, **C** H&E-stained inflammatory cell infiltration, **D** F4/80-stained immunofluorescence, **E** KIM-1 immunostaining, **F** picrosirius red-stained and **G** Masson's trichrome-stained kidney sections (taken at $\times 400$ magnification) show the extent of **B** peritubular capillary density; **C** kidney structural changes, protein cast formation (arrow), tubular dilation (*) as well as inflammatory cell aggregates (#); **D** macrophage (green-staining) infiltration in sections that were counterstained with collagen IV (red-staining); **E** KIM-1 (brown staining)-associated tubular epithelial damage; **F** red-stained tubulointerstitial; and **G** blue-stained glomerular matrix deposition within the kidney in each group studied. Scale bar = 100 μ m in each case. **H–M** Also shown is the semi-quantification of **H** CD31⁺ capillary density/field; **I** inflammatory cell; and **J** macrophage infiltration within the kidney; **K** kidney proximal tubular damage; **L** interstitial kidney fibrosis; or **M** glomerulosclerosis, expressed as **H, I, J, L, M** mean \pm SEM or **K** median \pm IQR per field analysed, from $n = 8$ non-overlapping fields of view; from $n = 7$ – 8 mice per group. * $p < 0.05$, ** $p < 0.01$, *** $p < 0.001$ vs the NDW control group; # $p < 0.05$, ## $p < 0.01$, ### $p < 0.001$ vs the HS alone group; * $p < 0.05$ vs the HS + BM-MSC-eGFP group; ** $p < 0.01$, *** $p < 0.001$ vs the HS + Perindopril-treated group; as determined using **H, J, K, L** a one-way ANOVA and Tukey's *post-hoc* test or **I, M** a non-parametric Kruskal–Wallis test with Dunn's *post-hoc* analysis

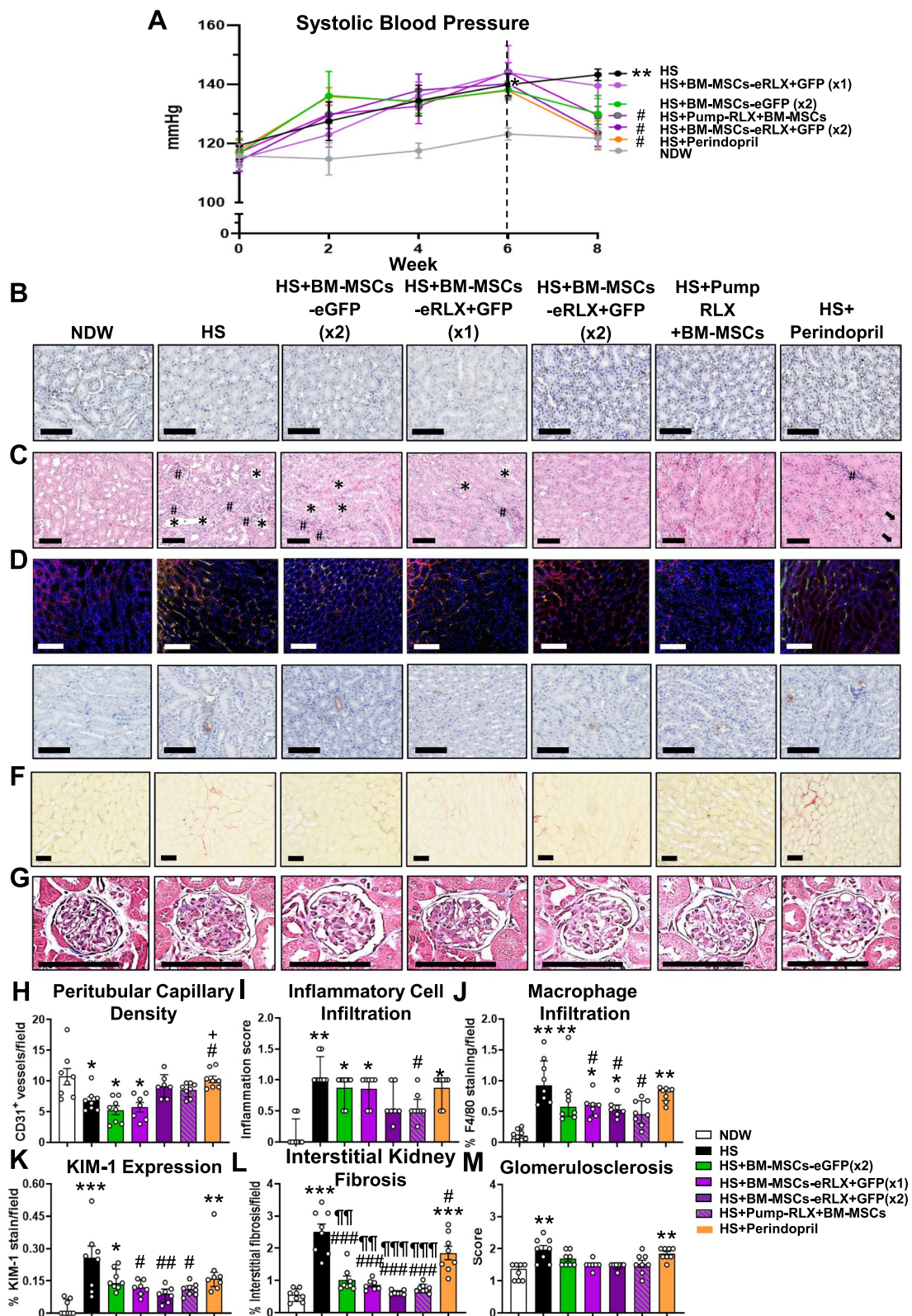


Fig. 5 (See legend on previous page.)

BM-MSCs-eRLX + GFP after 2-to-6 weeks of treatment. However, SBP levels in the BM-MSCs-eRLX + GFP-treated group remained similar to that of their HS-fed counterparts from weeks 16–47 post-treatment cessation. Remarkably, interstitial kidney fibrosis levels were still suppressed in the BM-MSCs-eRLX + GFP-treated group (0.4–1.0% per field) after 9-months of treatment cessation, and were not different to that measured from NDW-fed mice (Fig. 8C).

NDW-fed mice did not have any significant pathological abnormalities at 59-weeks of age, but presented with an age-induced subcapsular spindle cell hyperplasia (adrenal gland), diffuse vacuolar changes and centrilobar hepatocellular lipidosis (liver) (Fig. 8D). Similarly, no major abnormalities were observed in age-matched HS-fed mice and HS-fed mice treated BM-MSCs-eRLX + GFP ($\times 2$). However, these mice presented with the same minor abnormalities that were detected in NDW-fed control mice, and $n=2$ BM-MSCs-eRLX + GFP ($\times 2$)-treated mice had mild multifocal interstitial lymphoplasmacytic infiltrations, whilst $n=1$ of these two BM-MSCs-eRLX + GFP ($\times 2$)-treated mice also had mild multifocal cystically dilated renal tubules and mild early hydronephrosis (kidney).

Discussion

For the first time, a lentiviral vector that contained an expression cassette for an anti-fibrotic hormone, relaxin (RLX) [6, 16] and GFP (as a fluorescent reporter), was stably used to transduce human BM-MSCs. Remarkably, our data highlighted that these BM-MSCs-eRLX + GFP produced biologically active and therapeutic RLX levels in vitro (~ 30 ng/ml after 3–7-days in culture) and in vivo (~ 1 -2 ng/ml after once-weekly injections over 2-weeks), and retained their differentiation and proliferative capacity compared to naïve BM-MSCs in vitro. In experimental models of IRI-induced AKI or HS-loading induced CKD, BM-MSCs-eRLX + GFP could be identified in the kidneys up to 7–14-days post-transplantation, with a

trend towards improved engraftment capacity compared to naïve BM-MSCs. This enhanced viability and engraftment of BM-MSCs-eRLX + GFP to the injured site by the presence of RLX, in turn, prolonged the anti-fibrotic properties of RLX (which has a short in vivo half-life of ~ 4 –8 h [31, 32]) within the injured kidney for up to 14-days following a single injection.

Interestingly, both BM-MSCs-eGFP and BM-MSCs-eRLX GFP were found to be widely distributed in the injured kidney, heart lung, spleen and liver of IRI mice from 5-to-14-days post-transplantation, but were selectively found in the kidneys of HS-fed mice from 7-to-14-days post-administration. These findings extended our previous findings in IRI mice [34], which found that BM-MSCs-eGFP migrated to the injured kidney within 24 h of transplantation and remained in the kidney after 72 h. This differential homing and distribution of the i.v.-injected MSCs could be impacted by various factors related to the specific pathophysiology, inflammatory response to injury and microenvironment of the different models studied, but are consistent with previous reports of the biodistribution of MSCs in murine models of acute kidney injury [51, 52]. Notably though, whilst BM-MSCs-eGFP demonstrated anti-hypertensive and anti-fibrotic effects in the preclinical models established, it was clearly evident that the added effects of RLX with BM-MSCs provided broader (anti-inflammatory, anti-remodelling and tissue-reparative) renoprotection compared to the effects of BM-MSCs alone or the current standard of care medication, perindopril. Importantly, these broad renoprotective effects of BM-MSCs-eRLX + GFP were maintained in the presence of perindopril treatment, and even up to 9-months post-treatment cessation, suggesting that these combination cell-based treatments could effectively maintain their efficacy as adjunct therapies to clinically-used ACEi in the absence of any adverse side-effects.

Our study unveiled several noteworthy findings that significantly add to the current understanding of the application of genetically-engineered MSC-based

(See figure on next page.)

Fig. 6 The effects of HS and the treatments evaluated on additional measures that control the rate of kidney fibrosis and on kidney function. **A, B** Representative images of **A** α -SMA immunostaining and **B** pSmad2 immunofluorescence staining within kidney sections (at $\times 400$ magnification) show the extent of **A** brown-stained interstitial myofibroblast accumulation and; **B** red-stained pSmad2 expression in each of the groups evaluated, respectively. Scale bar = **A** 100 μ m or **B** 50 μ m. **C** A representative gelatin zymography shows the extent of glycosylated (G), latent (L) and active (A) MMP-9 (gelatinase B) and MMP-2 (gelatinase A) levels within the kidneys of each of the groups evaluated. An additional $n=4$ samples per group were run on separate zymographs, which produced similar results. **D-F** Also shown are the mean \pm SEM % **D** α -SMA staining/field; **E** TGF- β 1 expression levels (determined by ELISA analysis of kidney protein extracts); or **F** % pSmad2 staining/field (relative to that in the NDW control group), from $n=8$ non-overlapping fields of view or 30 glomeruli per section analysed; from $n=6$ –8 mice per group—for the analysis of tubulointerstitial fibrosis, glomerular matrix deposition, interstitial myofibroblast accumulation and pSmad2 staining. **G-J** Additionally shown are the mean \pm SEM **G** relative OD A-MMP-9; **H** relative OD A-MMP-2; **I** proteinuria; or **J** creatinine clearance; from $n=6$ –7 mice per group. * $p < 0.05$, ** $p < 0.01$, *** $p < 0.001$ vs the NDW control group; # $p < 0.05$, ## $p < 0.01$ vs the HS alone group; ** $p < 0.01$ vs the HS + Perindopril-treated group; as determined **D, E, F, I, J** using a one-way ANOVA and Tukey's *post-hoc* test or **G, H** a non-parametric Kruskal–Wallis test with Dunn's *post-hoc* analysis

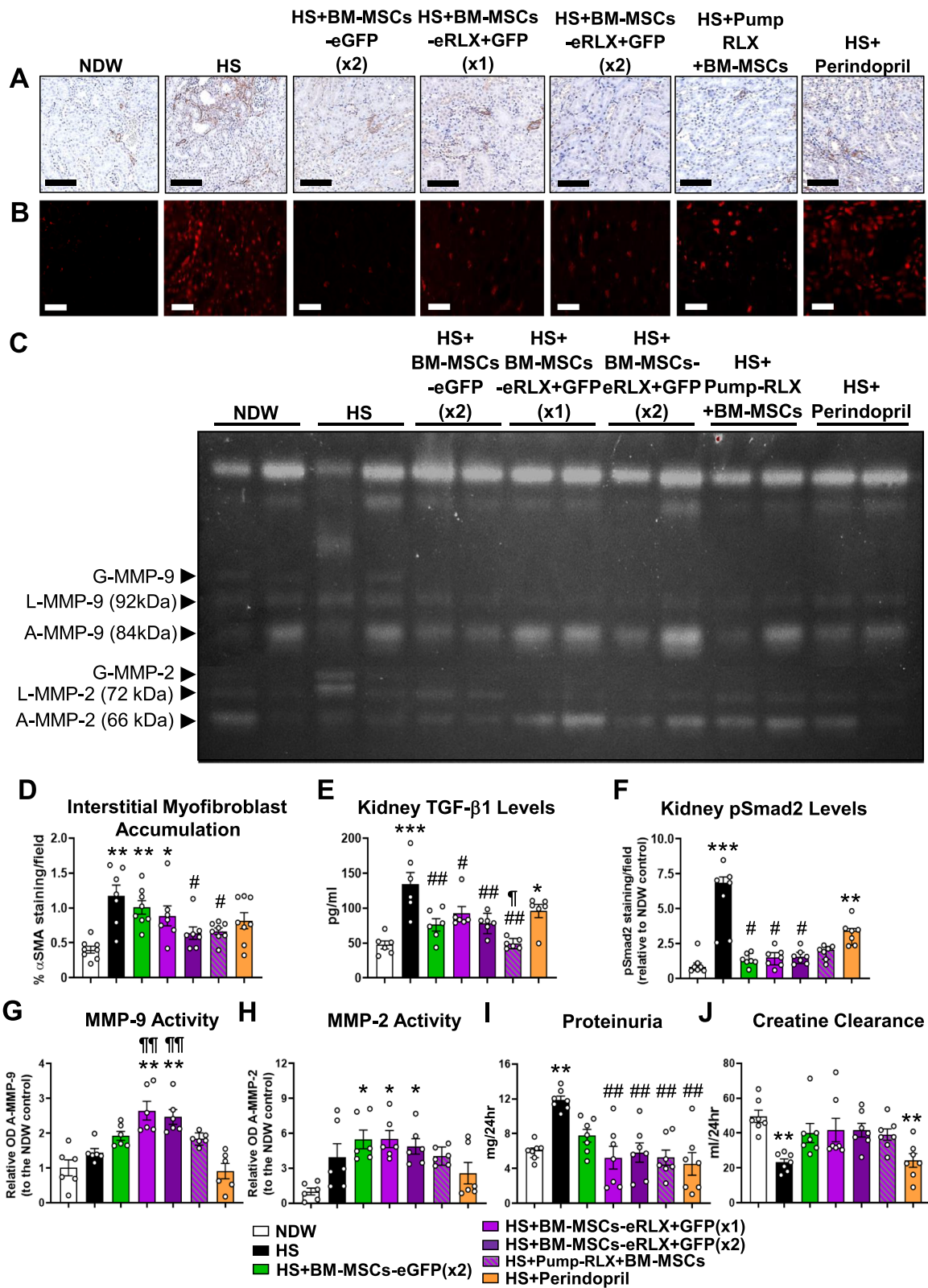


Fig. 6 (See legend on previous page.)

therapies for treating CKD. Strikingly, a single i.v injection of BM-MSCs-eRLX+GFP significantly attenuated the IRI-induced kidney inflammation, tubular epithelial injury, interstitial kidney fibrosis and glomerulosclerosis after 7-days. Furthermore, a once-weekly i.v injection of BM-MSCs-eRLX+GFP over 2-weeks, significantly attenuated or normalised the HS-induced SBP, vascular endothelial and tubular epithelial damage, kidney inflammation, tubulointerstitial kidney fibrosis and glomerulosclerosis over a 14-day period. Most importantly, in addition to ameliorating factors that contribute to aberrant ECM/collagen accumulation (such as BP, epithelial tubular damage, immune cell infiltration, pro-inflammatory cytokine expression, pro-fibrotic TGF- β 1/pSmad2 activity and myofibroblast accumulation), the anti-fibrotic effects of BM-MSCs-eRLX+GFP was mediated via their promotion of collagen-degrading gelatinase activity. This would be expected to facilitate the degradation of established collagen, consistent with the reported collagen-degrading effects of RLX [45, 53], an effect that would not likely be provoked by BM-MSCs engineered to express other factors [12–15] that would only attenuate kidney damage-induced ECM production and deposition. Furthermore, these renoprotective effects of BM-MSCs-eRLX+GFP also led to the ability of these cells to normalise the HS-induced renal functional impairment after 14-days of treatment. Hence, this study importantly showed that the lentiviral transduction of RLX to human BM-MSCs did not compromise the broad therapeutic effects of RLX [6, 16]. Based on these collective findings, and those from a separate study that genetically-engineered a murine skeletal myoblast cell line to express RLX [54], it is proposed that the presence of RLX both reduced the fibrotic environment into which BM-MSCs-eRLX+GFP were administered into, and increased the number of viable BM-MSCs that could then exert greater therapeutic and reparative effects over that of BM-MSCs-eGFP alone.

As confirmation of this, BM-MSCs-eGFP alone failed to affect the IRI- or HS-induced inflammatory cell infiltration, tubular damage, glomerulosclerosis or interstitial

myofibroblast accumulation when administered over the corresponding treatment period as BM-MSCs-eRLX+GFP in each model. Furthermore, despite exerting anti-hypertensive properties [28, 41] that have been shown to be mediated via the suppression of inflammatory factors that contribute to BP [41] or through their suppression of renin-angiotensin system components (angiotensin II, ACE, AT1 receptor) [55], BM-MSCs-eGFP alone did not ameliorate the HS-induced SBP to the same extent as BM-MSCs-eRLX+GFP. Similarly, the combined effects of BM-MSCs and RLX provided broader renoprotection over a current standard of care treatment for hypertensive CKD, perindopril, in HS-fed mice, which failed to affect the HS-induced inflammatory cell infiltration, tubular damage, glomerulosclerosis, gelatinase activity or creatinine clearance. These findings are consistent with previous studies that demonstrated the more rapid and broader renoprotective effects of BM-MSCs and RLX when combined, compared to perindopril in 1 K/DOCA/salt-hypertensive mice [28]. Given the slow-acting anti-fibrotic efficacy of ACEi [27, 56, 57], which induce anti-hypertensive and anti-inflammatory effects but do not resolve existing fibrosis, it is proposed that BM-MSCs-eRLX+GFP could even be employed as a stand-alone therapy for CKD, which induced similar anti-hypertensive effects to that of ACEi but broader renoprotection and rapid restoration of kidney functional impairment over these currently-used therapies.

It was also noted that a single i.v injection of BM-MSCs-eRLX+GFP abolished the HS-induced tubulointerstitial kidney fibrosis, glomerulosclerosis and kidney functional impairment, and stimulated gelatinase activity beyond that measured in NDW-fed mice by 14-days post-administration, to an equivalent extent as once-weekly administration of BM-MSCs-eRLX+GFP over the 2-week treatment period evaluated. This was despite BM-MSCs-eRLX+GFP ($\times 1$) treatment having no significant effects on the HS-induced increase in SBP or tubular damage. These findings corroborated our previous studies in preclinical models of kidney [28, 39] and lung [58–60] disease, which indicated that the targeting

(See figure on next page.)

Fig. 7 BM-MSCs-eRLX+GFP maintained their therapeutic efficacy in the presence of perindopril (ACEi). (A) Shown is the mean \pm SEM SBP, from week-0 to week-8 of the HS-induced model established and treated; from $n=8$ mice per group shown. **B-E** Representative images of **B** H&E-stained inflammatory cell infiltration, **C** picrosirius red-staining, **D** Masson's trichrome-staining, and **E** α -SMA immunostaining (taken at $\times 400$ magnification) show the extent of **B** kidney structural changes, tubular dilation (*) as well as inflammatory cell aggregates (#); **C** red-stained tubulointerstitial fibrosis; **D** blue-stained glomerular matrix deposition; and **E** brown-stained interstitial myofibroblast accumulation in each of the groups evaluated, respectively. Scale bar = 100 μ m in each case. **F-K** Also shown is the median \pm IQR **F** inflammatory cell infiltration; or (H) glomerulosclerosis score; or the mean \pm SEM **G** % interstitial kidney fibrosis staining per field analysed; **I** % α -SMA staining/field; **J** proteinuria (mg/24 h); or **K** creatinine clearance (ml/24 h); from $n=7-8$ mice per group. * $p < 0.05$, ** $p < 0.01$, *** $p < 0.001$ vs the NDW control group; # $p < 0.05$, ## $p < 0.01$; ### $p < 0.001$ vs the HS alone group; * $p < 0.05$, ** $p < 0.01$, *** $p < 0.001$ vs the HS + Perindopril-treated group; as determined using **G, I, J, K** a one-way ANOVA and Tukey's *post-hoc* test or **F, H** a non-parametric Kruskal–Wallis test with Dunn's *post-hoc* analysis

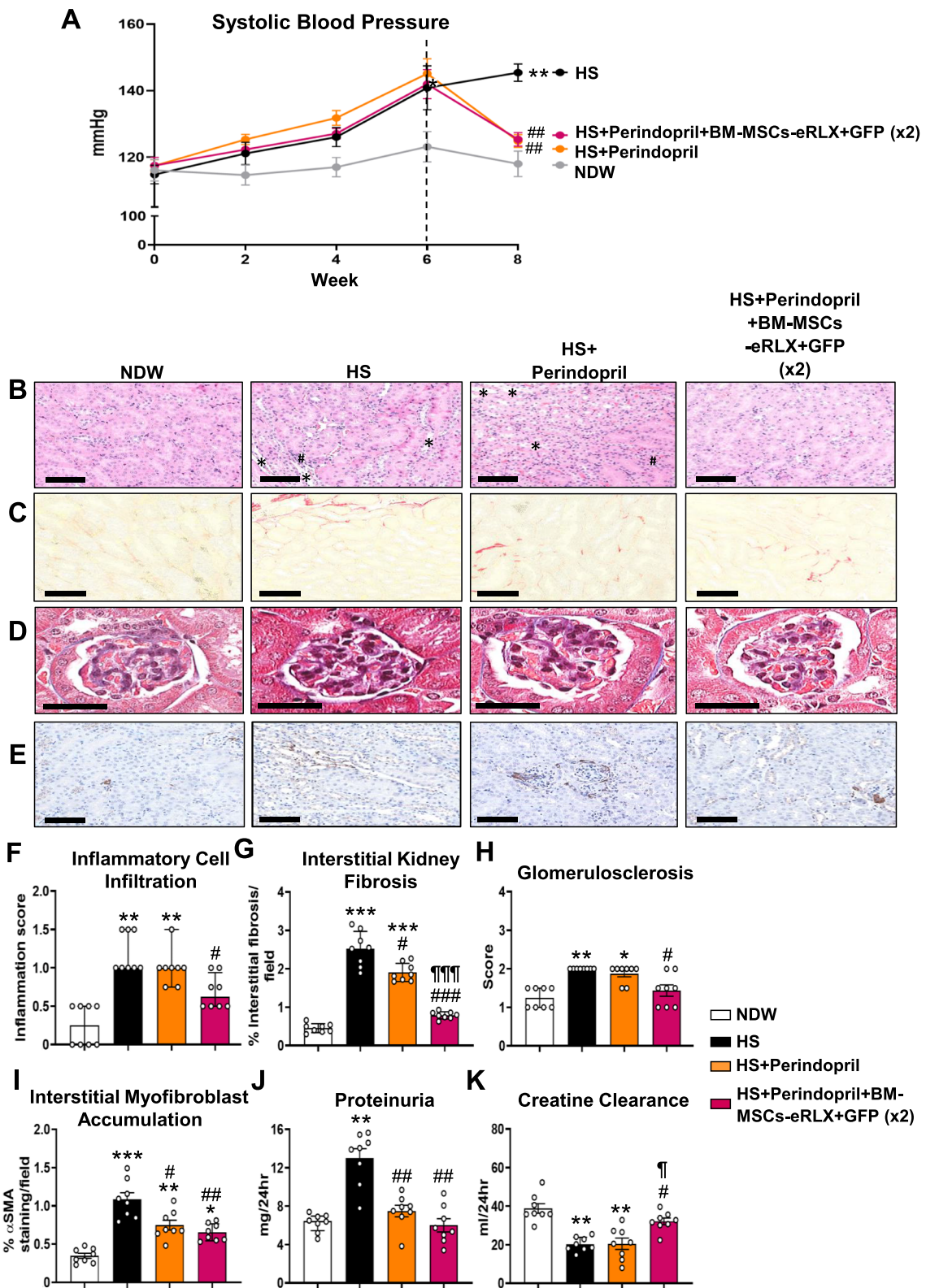


Fig. 7 (See legend on previous page.)

of injury-induced fibrosis progression is likely to have a larger impact on alleviating kidney dysfunction compared to other pathological features of disease progression. Indeed, it has been determined that fibrosis is a major contributor to proteinuria [61], which may explain why all treatments evaluated that displayed anti-fibrotic effects, including perindopril which induced modest anti-fibrotic efficacy in HS-fed mice, were able to blunt or significantly reduce the HS-induced proteinuria. On the other hand, the regulation of creatinine clearance, which can be used to estimate GFR, requires the targeting of several disease-related pathologies [62], which perindopril failed to address in the current study. Hence, these findings highlighted the added benefit of engineering BM-MSCs with the anti-fibrotic properties of RLX.

Conclusions

In summary, this study has showcased a revolutionary strategy for genetically engineering MSCs with an anti-fibrotic agent that promotes the MMP-induced resolution of established ECM. In doing so, it has highlighted the therapeutic potential of RLX-producing BM-MSCs as a novel treatment option for AKI and CKD. These engineered cells retained the characteristics of their naïve counterparts, but in acquiring the added presence of RLX, displayed enhanced viability post-transplantation and effectively attenuated or normalised injury-induced kidney inflammation, tubular injury, fibrosis and functional impairment, particularly when administered once-weekly over a 2-week period. Not only do these engineered cells provide a more clinically-feasible means of delivering the therapeutic impact of this combination therapy to human CKD patients, as BM-MSCs [6, 8, 9] RLX [16] or BM-MSCs-eRLX + GFP have demonstrated an excellent safety profile, this bodes well for the fast-tracking of BM-MSCs-eRLX + GFP as a clinically-viable treatment option for CKD.

(See figure on next page.)

Fig. 8 Evaluation of the long-term efficacy and safety of BM-MSCs-eRLX + GFP. **A** Shown is the mean \pm SEM SBP, as measured once-fortnightly from week-0 to week-8, and then once-monthly from week-8 to week-47, from the HS-induced model established and treated; from NDW (n = 3) or HS (n = 3)-fed mice, and HS + BM-MSCs-eRLX + GFP ($\times 2$)-treated mice (n = 4). **B** Representative images of Masson's trichrome-staining show the extent of blue-stained tubulointerstitial fibrosis in each of the groups studied. Scale bar = 200 μ m. **C** Also shown is the mean \pm SEM % interstitial kidney fibrosis staining per field analysed from each group evaluated; from n = 8 non-overlapping fields of view analysed; from n = 3–4 mice per group. *p < 0.05, **p < 0.01 vs the NDW control group; #p < 0.05 vs the HS alone group; as determined using a two-way ANOVA (A) or one-way ANOVA (C) and Tukey's *post-hoc* test in each case. **D** A summary of the pathological assessment of the three groups of mice evaluated, 9 months after BM-MSCs-eRLX + GFP ($\times 2$) had stopped. †n = 2 out of 6 HS-fed mice injected with BM-MSC-eRLX + GFP ($\times 2$) started to chew their tails after the i.v.-injection of cells, and had to be humanely killed shortly thereafter—so could not be assessed. 'No abnormalities' implies that no significant abnormalities were detected in these mice. However: ^an = 1 HS-fed mouse and n = 2 HS + BM-MSCs-eRLX + GFP-treated mice had mild multifocal interstitial lymphoplasmacytic infiltrations, and n = 1 HS + BM-MSCs-eRLX + GFP-treated mouse had mild multifocal cystically dilated renal tubules and mild early renal hydronephrosis; ^ball mice had evidence of subcapsular spindle cell hyperplasia (adrenal gland); ^cseveral mice from each group had focal to multifocal mineralisation of the right ventricle; ^dseveral mice from each of the HS-fed groups had focal bronchoalveolar adenoma (lung); ^ealmost all mice had age-related diffuse glycogen-type vacuolar changes and mild, diffuse centrilobular hepatocellular lipidosis. The organ weights presented are expressed as the mean \pm SEM; from n = 3–4 mice per group (as denoted by the numbers in the square brackets)

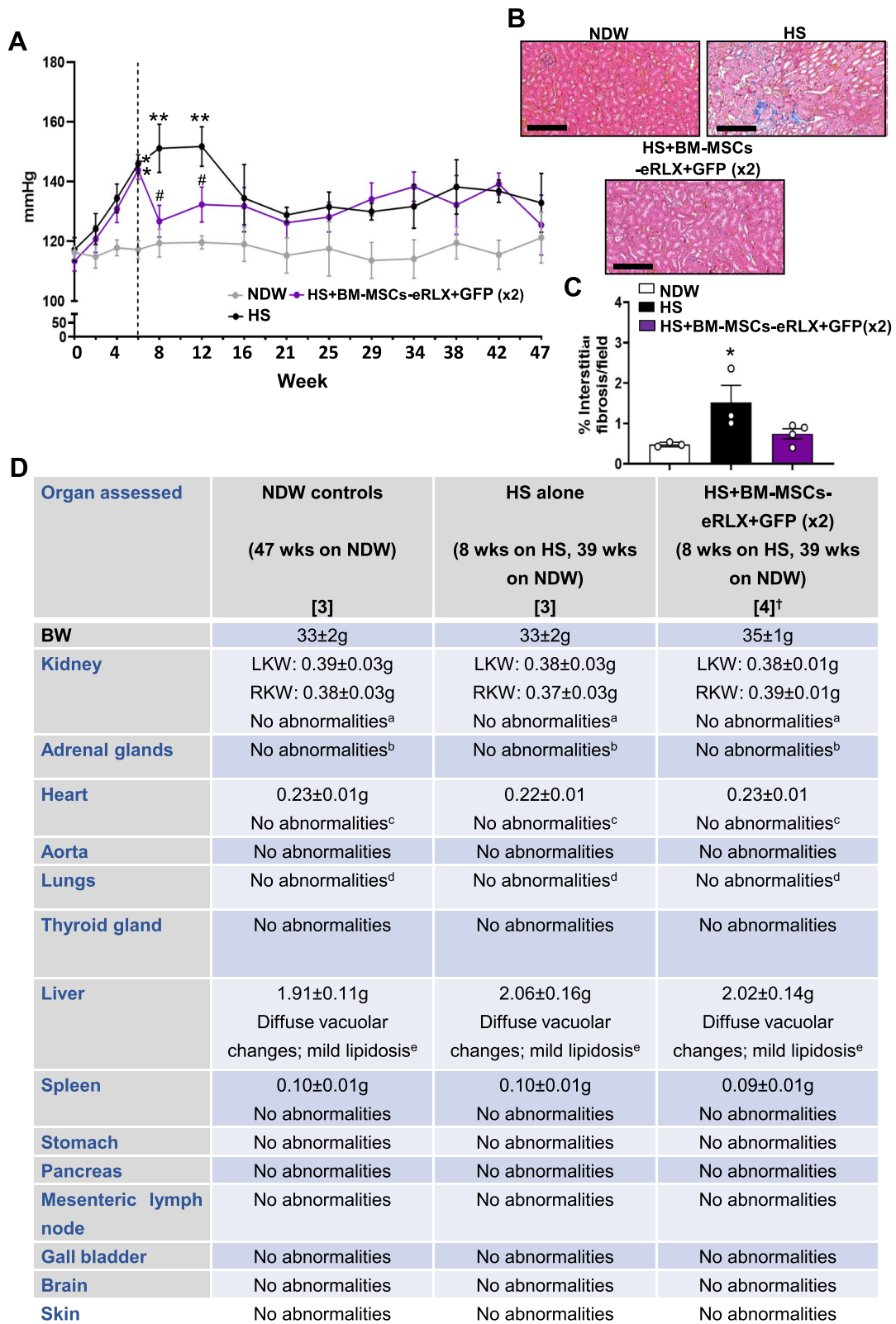


Fig. 8 (See legend on previous page.)

Abbreviations

CKD	Chronic kidney disease
BM-MSCs	Bone marrow-derived mesenchymal stromal cells
RLX	Human relaxin-2
BM-MSCs-eGFP	BM-MSCs-expressing green fluorescent protein
BM-MSCs-eRLX + GFP	BM-MSCs-expressing human relaxin-2 + green fluorescent protein
IRI	Ischemia reperfusion injury (IRI)
HS	High salt
ECM	Extracellular matrix
MMP	Matrix metalloproteinase
ACE	Angiotensin converting enzyme
CFU-F	colony-forming unit-fibroblasts
CD	Cluster of differentiation
HLA-DR	Human leukocyte antigen DR isotype
α -MEM	α -Minimal essential media
FBS	Fetal bovine serum
P	Passage
LV	Lentivirus
EF1A	Eukaryotic translation elongation factor-1 α
MOI	Multiplicity of infection
RXFP1	Relaxin Family Peptide Receptor 1
DAPI	4',6-diamidino-2-phenylindole
FABP4	Fatty acid binding protein 4
NDW	Normal drinking water
SBP	Systolic blood pressure
gDNA	Genomic DNA
PCR	Polymerase chain reaction
OCT	Optimal cutting temperature
KIM	Kidney injury molecule
SMA	Smooth muscle actin
IgG	Immunoglobulin G
FACS	Fluorescence-activated cell sorting
ELISA	Enzyme-linked immunosorbent assay
MCP	Monocyte chemoattractant protein
TNF	Tumour necrosis factor
IL	Interleukin
TGF	Transforming growth factor
OD	Optical density
IGFBP	Insulin-like growth factor binding protein
uPAR	Urokinase-type plasminogen activation receptor
PDGF-AA	platelet-derived growth factor containing two A subunits
VEGF	Vascular endothelial growth factor
Smad2	Mothers against decapentaplegic homolog 2

Supplementary Information

The online version contains supplementary material available at <https://doi.org/10.1186/s13287-024-03992-x>.

Additional file 1.

Acknowledgements

We are grateful to Mr. Joseph Chen (Department of Anatomy and Developmental Biology, Monash University) for assisting Dr. Yifang Li to design the lentivirus vector construct that contained bicistronically expressed human relaxin-2 cDNA and enhanced green fluorescent protein (EGFP) gene under an EF1A promoter (pLV-EF1A-hRLN2-EGFP); Mrs Sheetal Saini (Department of Pharmacology, Monash University) for assistance with BM-MSC culture; the Monash Histology Platform for the assistance provided on tissue processing, sectioning and staining; the Monash Micro Imaging Platform for their assistance with fluorescence microscopy imaging; and Cerberus Science (Pathology Services) for assessing the various mouse organs associated with the safety study reported. The Authors declare that they have not used any AI-generated work in this manuscript.

Author contributions

C.S.S. and S.D.R. acquired funding for the study, designed and coordinated the reported studies, supervised students and performed data analysis. Y.L. generated and characterised BM-MSCs-GFP and BM-MSCs-RLX + GFP in vitro with the assistance of G.S., R.W.K.L. and P.M., and completed all the in vivo studies reported on the high salt model. A.H. completed the in vivo studies on the ischemia reperfusion injury model under the supervision of C.S.S. and S.D.R. whilst M.M.W. completed the in vivo studies on evaluating the effects of BM-MSCs-RLX + GFP in the presence of an ACE inhibitor under the supervision of C.S.S. and Y.L. B.R.S.B. performed tail vein injections of BM-MSCs-GFP or BM-MSCs-RLX + GFP into the appropriate animals. I.E.O.P. extracted and analysed the BM-MSCs-exosomes under the supervision of M.P.D.B. Z.D. and T.Z. assisted Y.L. and contributed to confirming that BM-MSCs-GFP and BM-MSCs-RLX + GFP homed to the kidneys of mice following ischemia reperfusion injury or high salt-feeding. R.E.W. and J.M.P. contributed to the acquisition of funding for the outlined studies, provided reagents and supervised students. Y.L. and C.S.S. wrote the initial draft of the manuscript, which all other Authors read and edited. All Authors have agreed upon the published version of the manuscript.

Funding

This work was supported by Monash Graduate Scholarships to Y.L. and I.E.O.P.; a National Health & Medical Research Council (NHMRC) of Australia Project Grant (GNT1156446) to C.S.S., S.D.R. and R.E.W.; a NHMRC Ideas Grant (GNT2019014) to C.S.S., S.D.R., Y.L., J.M.P. and R.E.W.; and a Monash Biomedicine Discovery Fellowship to C.S.S.

Availability of data and materials

The data supporting the findings from this study are available within the manuscript and its Supplementary Information. Any remaining raw data are archived in a Monash University repository and will be available from the corresponding authors upon reasonable request. Some data may not be available because of privacy or ethical restrictions.

Declarations

Ethics approval and consent to participate

The work performed on the IRI model was approved (on 04/08/2022) under the application: Monash Animal Research Platform (MARF)/2022/29417, titled 'Cell and diet-based therapies in experimental kidney disease', by the Monash University Animal Ethics Committee. The work performed on the HS model was approved (on 23/08/2021) under the application: MARF/2021/30019, titled 'Evaluation of engineered mesenchymal stem cells in an experimental model of hypertension', by the Monash University Animal Ethics Committee.

Consent for publication

Not applicable.

Competing interests

All authors have no conflicts of interest to disclose.

Author details

¹Cardiovascular Disease Program, Monash Biomedicine Discovery Institute, Monash University, Clayton, VIC 3800, Australia. ²Development and Stem Cells Program, Monash Biomedicine Discovery Institute, Monash University, Clayton, VIC 3800, Australia. ³Department of Pharmacology, Monash University, Clayton, VIC 3800, Australia. ⁴Department of Anatomy and Developmental Biology, Monash University, Clayton, VIC 3800, Australia. ⁵Department of Medicine (Alfred Hospital), Central Clinical School, Monash University, Melbourne, VIC 3004, Australia. ⁶Adelaide Centre for Epigenetics, School of Biomedicine, The University of Adelaide, Adelaide, SA 5005, Australia. ⁷The South Australian Immunogenomics Cancer Institute, The University of Adelaide, Adelaide, SA 5005, Australia. ⁸Department of Biochemistry and Pharmacology, The University of Melbourne, Parkville, VIC 3010, Australia.

Received: 6 August 2024 Accepted: 9 October 2024

Published: 23 October 2024

References

- Levey AS, Eckardt K-U, Tsukamoto Y, Levin A, Coresh J, Rossert J, et al. Definition and classification of chronic kidney disease: a position statement from kidney disease: improving global outcomes (KDIGO). *Kidney Int.* 2005;67(6):2089–100.
- Zoccali C, Vanholder R, Massy ZA, Ortiz A, Sarafidis P, Dekker FW, et al. The systemic nature of CKD. *Nat Rev Nephrol.* 2017;13(6):344–58.
- Eddy AA. Overview of the cellular and molecular basis of kidney fibrosis. *Kidney Int Suppl.* 2014;4(1):2–8.
- Klinkhammer BM, Goldschmeding R, Floege J, Boor P. Treatment of renal fibrosis - Turning challenges into opportunities. *Adv Chronic Kidney Dis.* 2017;24(2):117–29.
- English K. Mechanisms of mesenchymal stromal cell immunomodulation. *Immunol Cell Biol.* 2013;91(1):19–26.
- Li Y, Ricardo SD, Samuel CS. Enhancing the therapeutic potential of mesenchymal stromal cell-based therapies with an anti-fibrotic agent for the treatment of chronic kidney disease. *Int J Mol Sci.* 2022;23(11):6035.
- Perico N, Casiraghi F, Remuzzi G. Clinical translation of mesenchymal stromal cell therapies in nephrology. *J Am Soc Nephrol.* 2018;29(2):362–75.
- Makhlough A, Shekarchian S, Moghadasali R, Einollahi B, Dastgheib M, Janbabaee G, et al. Bone marrow-mesenchymal stromal cell infusion in patients with chronic kidney disease: a safety study with 18 months of follow-up. *Cytotherapy.* 2018;20(5):660–9.
- Makhlough A, Shekarchian S, Moghadasali R, Einollahi B, Hosseini SE, Jaroughi N, et al. Safety and tolerability of autologous bone marrow mesenchymal stromal cells in ADPKD patients. *Stem Cell Res Ther.* 2017;8(1):116.
- Skyler JS, Fonseca VA, Segal KR, Rosenstock J. Allogeneic mesenchymal precursor cells in type 2 diabetes: a randomized, placebo-controlled, dose-escalation safety and tolerability pilot study. *Diabetes Care.* 2015;38(9):1742–9.
- Packham DK, Fraser IR, Kerr PG, Segal KR. Allogeneic mesenchymal precursor cells (MPC) in diabetic nephropathy: a randomized, placebo-controlled, dose escalation study. *EBioMedicine.* 2016;12:263–9.
- Wang B, Yao K, Huuskas BM, Shen HH, Zhuang J, Godson C, et al. Mesenchymal stem cells deliver exogenous microRNA-let7c via exosomes to attenuate renal fibrosis. *Mol Therap.* 2016;24(7):1290–301.
- Burchfield JS, Iwasaki M, Koyanagi M, Urbich C, Rosenthal N, Zeiher AM, et al. Interleukin-10 from transplanted bone marrow mononuclear cells contributes to cardiac protection after myocardial infarction. *Circ Res.* 2008;103(2):203–11.
- Jin S, Li H, Han M, Ruan M, Liu Z, Zhang F, et al. Mesenchymal stem cells with enhanced Bcl-2 expression promote liver recovery in a rat model of hepatic cirrhosis. *Cell Physiol Biochem.* 2016;40(5):1117–28.
- Beckermann BM, Kallifatidis G, Groth A, Frommhold D, Apel A, Mattern J, et al. VEGF expression by mesenchymal stem cells contributes to angiogenesis in pancreatic carcinoma. *Br J Cancer.* 2008;99(4):622–31.
- Samuel CS, Bennett RG. Relaxin as an anti-fibrotic treatment: perspectives, challenges and future directions. *Biochem Pharmacol.* 2022;197:114884.
- Garber SL, Mirochnik Y, Brecklin CS, Unemori EN, Singh AK, Slobodskoy L, et al. Relaxin decreases renal interstitial fibrosis and slows progression of renal disease. *Kidney Int.* 2001;59(3):876–82.
- Garber G, Mirochnik Y, Brecklin CS, Slobodskoy L, Arruda JA, Dunea G. Effect of relaxin in two models of renal mass reduction. *Am J Nephrol.* 2003;23(1):8–12.
- McDonald GA, Sarkar P, Rennke H, Unemori E, Kalluri R, Sukhatme VP. Relaxin increases ubiquitin-dependent degradation of fibronectin in vitro and ameliorates renal fibrosis in vivo. *Am J Physiol Renal Physiol.* 2003;285(1):F59–67.
- Lekgabe ED, Kiriazis H, Zhao C, Xu Q, Moore SL, Su Y, et al. Relaxin reverses cardiac and renal fibrosis in spontaneously hypertensive rats. *Hypertension.* 2005;46(2):412–8.
- Danielson LA, Welford A, Harris A. Relaxin improves renal function and histology in aging Munich Wistar rats. *J Am Soc Nephrol.* 2006;17(5):1325–33.
- Hewitson TD, Ho WY, Samuel CS. Antifibrotic properties of relaxin: in vivo mechanism of action in experimental renal tubulointerstitial fibrosis. *Endocrinology.* 2010;151(10):4938–48.
- Sasser JM, Molnar M, Baylis C. Relaxin ameliorates hypertension and increases nitric oxide metabolite excretion in angiotensin II but not N(omega)-nitro-L-arginine methyl ester hypertensive rats. *Hypertension.* 2011;58(2):197–204.
- Yoshida T, Kumagai H, Kohsaka T, Ikegaya N. Relaxin protects against renal ischemia-reperfusion injury. *Am J Physiol Renal Physiol.* 2013;305(8):F1169–76.
- Yoshida T, Kumagai H, Kohsaka T, Ikegaya N. Protective effects of relaxin against cisplatin-induced nephrotoxicity in rats. *Nephron Exp Nephrol.* 2014;128(1–2):9–20.
- Wang D, Luo Y, Myakala K, Orlicky DJ, Dobrinskikh E, Wang X, et al. Sere-laxin improves cardiac and renal function in DOCA-salt hypertensive rats. *Sci Rep.* 2017;7(1):9793.
- Samuel CS, Bodaragama H, Chew JY, Widdop RE, Royce SG, Hewitson TD. Sere-laxin is a more efficacious antifibrotic than enalapril in an experimental model of heart disease. *Hypertension.* 2014;64(2):315–22.
- Li Y, Shen M, Ferens D, Broughton BRS, Murthi P, Saini S, et al. Combining mesenchymal stem cells with sere-laxin provides enhanced renoprotection against 1K/DOCA/salt-induced hypertension. *Br J Pharmacol.* 2021;178(5):1164–81.
- Huuskas BM, Wise AF, Cox AJ, Lim EX, Payne NL, Kelly DJ, et al. Combination therapy of mesenchymal stem cells and sere-laxin effectively attenuates renal fibrosis in obstructive nephropathy. *FASEB J.* 2015;29(2):540–53.
- Seibold JR, Korn JH, Simms R, Clements PJ, Moreland LW, Mayes MD, et al. Recombinant human relaxin in the treatment of scleroderma. A randomized, double-blind, placebo-controlled trial. *An Int Med.* 2000;132(11):871–9.
- Chen SA, Perlman AJ, Spanski N, Peterson CM, Sanders SW, Jaffe R, et al. The pharmacokinetics of recombinant human relaxin in nonpregnant women after intravenous. *Intravag Intracerv Administr Pharm Res.* 1993;10(6):834–8.
- Dahlke M, Halabi A, Canadi J, Tsubouchi C, Machineni S, Pang Y. Pharmacokinetics of sere-laxin in patients with severe renal impairment or end-stage renal disease requiring hemodialysis: A single-dose, open-label, parallel-group study. *J Clin Pharmacol.* 2016;56(4):474–83.
- Chawla LS, Eggers PW, Star RA, Kimmel PL. Acute kidney injury and chronic kidney disease as interconnected syndromes. *New Eng J Med.* 2014;371(1):58–66.
- Wise AF, Williams TM, Kiewiet MB, Payne NL, Siatskas C, Samuel CS, et al. Human mesenchymal stem cells alter macrophage phenotype and promote regeneration via homing to the kidney following ischemia-reperfusion injury. *Am J Physiol Renal Physiol.* 2014;306(10):F1222–35.
- Badawi A, Jefferson OC, Huuskas BM, Ricardo SD, Kerr PG, Samuel CS, et al. A novel approach to enhance the regenerative potential of circulating endothelial progenitor cells in patients with end-stage kidney disease. *Biomedicine.* 2002;10(4):883.
- Neugarten J, Golestaneh L. Influence of sex on the progression of chronic kidney disease. *Mayo Clin Proc.* 2019;94(7):1339–56.
- Samuel CS, Zhao C, Bathgate RAD, Bond CP, Burton MD, Parry LJ, et al. Relaxin deficiency in mice is associated with an age-related progression of pulmonary fibrosis. *FASEB J.* 2003;17(1):121–3.
- Beaini S, Saliba Y, Hajal J, Smayra V, Bakhos JJ, Joubran N, et al. VEGF-C attenuates renal damage in salt-sensitive hypertension. *J Cell Physiol.* 2019;234(6):9616–30.
- Gao XM, Tsai A, Al-Sharea A, Su Y, Moore S, Han LP, et al. Inhibition of the renin-angiotensin system post myocardial infarction prevents inflammation-associated acute cardiac rupture. *Cardiovascular Drugs Ther.* 2017;31(2):145–56.
- Alikhan MA, Jones CV, Williams TM, Beckhouse AG, Fletcher AL, Kett MM, et al. Colony-stimulating factor-1 promotes kidney growth and repair via alteration of macrophage responses. *Am J Path.* 2011;179(3):1243–56.
- Li Y, Chakraborty A, Broughton BRS, Ferens D, Widdop RE, Ricardo SD, et al. Comparing the renoprotective effects of BM-MSCs versus BM-MSC-exosomes, when combined with an anti-fibrotic drug, in hypertensive mice. *Biomed Pharmacother.* 2021;144:112256.

42. Maric C, Sandberg K, Hinojosa-Laborde C. Glomerulosclerosis and tubulointerstitial fibrosis are attenuated with 17beta-estradiol in the aging Dahl salt sensitive rat. *J Am Soc Nephrol*. 2004;15(6):1546–56.
43. Woessner JF Jr. Quantification of matrix metalloproteinases in tissue samples. *Methods Enzymol*. 1995;248:510–28.
44. Dominici M, Le Blanc K, Mueller I, Slaper-Cortenbach I, Marini F, Krause D, et al. Minimal criteria for defining multipotent mesenchymal stromal cells. *Int Soc Cell Therapy Posit Statem Cytother*. 2006;8(4):315–7.
45. Unemori EN, Amento EP. Relaxin modulates synthesis and secretion of procollagenase and collagen by human dermal fibroblasts. *J Biol Chem*. 1990;265(18):10681–5.
46. Unemori EN, Bauer EA, Amento EP. Relaxin alone and in conjunction with interferon-gamma decreases collagen synthesis by cultured human scleroderma fibroblasts. *J Invest Dermatol*. 1992;99(3):337–42.
47. Unemori EN, Pickford LB, Salles AL, Piercy CE, Grove BH, Erikson ME, et al. Relaxin induces an extracellular matrix-degrading phenotype in human lung fibroblasts in vitro and inhibits lung fibrosis in a murine model in vivo. *J Clin Invest*. 1996;98(12):2739–45.
48. Bell RJ, Eddie LW, Lester AR, Wood EC, Johnston PD, Niall HD. Relaxin in human pregnancy serum measured with an homologous radioimmunoassay. *Obstet Gynecol*. 1987;69(4):585–9.
49. Teerlink JR, Metra M, Felker GM, Ponikowski P, Voors AA, Weatherley BD, et al. Relaxin for the treatment of patients with acute heart failure (Pre-RELAX-AHF): a multicentre, randomised, placebo-controlled, parallel-group, dose-finding phase IIb study. *Lancet*. 2009;373(9673):1429–39.
50. Gallo G, Volpe M, Savoia C. Endothelial dysfunction in hypertension: Current concepts and clinical implications. *Front Med (Lausanne)*. 2021;8:798958.
51. Togel F, Yang Y, Zhang P, Hu Z, Westenfelder C. Bioluminescence imaging to monitor the in vivo distribution of administered mesenchymal stem cells in acute kidney injury. *Am J Physiol Renal Physiol*. 2008;295(1):F315–21.
52. Sanchez-Diaz M, Quinones-Vico MI, Sanabria de la Torre R, Montero-Vilchez T, Sierra-Sanchez A, Molina-Leyva A, et al. Biodistribution of mesenchymal stromal cells after administration in animal models and humans: A systematic review. *J Clin Med*. 2021;10(13):2925.
53. Bennett RG, Heimann DG, Singh S, Simpson RL, Tuma DJ. Relaxin decreases the severity of established hepatic fibrosis in mice. *Liver Int*. 2014;34(3):416–26.
54. Formigli L, Perna AM, Meacci E, Cinci L, Margheri M, Nistri S, et al. Paracrine effects of transplanted myoblasts and relaxin on post-infarction heart remodelling. *J Cell Mol Med*. 2007;115:1087–100.
55. de Oliveira-Sales EB, Nishi EE, Boim MA, Dolnikoff MS, Bergamaschi CT, Campos RR. Upregulation of AT1R and iNOS in the rostral ventrolateral medulla (RVLM) is essential for the sympathetic hyperactivity and hypertension in the 2K–1C Wistar rat model. *Am J Hypertens*. 2010;23(7):708–15.
56. Gross O, Beirowski B, Koepke ML, Kuck J, Reiner M, Addicks K, et al. Preemptive ramipril therapy delays renal failure and reduces renal fibrosis in COL4A3-knockout mice with Alport syndrome. *Kidney Int*. 2003;63(2):438–46.
57. Srivastava SP, Goodwin JE, Kanasaki K, Koya D. Inhibition of angiotensin-converting enzyme ameliorates renal fibrosis by mitigating DPP-4 level and restoring antifibrotic microRNAs. *Genes (Basel)*. 2020;11(2):211.
58. Royce SG, Miao YR, Lee M, Samuel CS, Treegar GW, Tang MLK. Relaxin reverses airway remodeling and airway dysfunction in allergic airways diseases. *Endocrinology*. 2009;150(6):2692–9.
59. Patel KP, Giraud AS, Samuel CS, Royce SG. Combining an epithelial repair factor and anti-fibrotic with a corticosteroid offers optimal treatment for allergic airways disease. *Br J Pharmacol*. 2016;173(12):2016–29.
60. Royce SG, Mao W, Lim R, Kelly K, Samuel CS. iPSC- and mesenchymalangioblast-derived mesenchymal stem cells provide greater protection against experimental chronic allergic airways disease compared with a clinically used corticosteroid. *FASEB J*. 2019;33(5):6402–11.
61. Kuusniemi AM, Lapatto R, Holmberg C, Karikoski R, Rapola J, Jalanko H. Kidneys with heavy proteinuria show fibrosis, inflammation, and oxidative stress, but no tubular phenotypic change. *Kidney Int*. 2005;68(1):121–32.
62. Sharma A, Sahasrabudhe V, Musib L, Zhang S, Younis I, Kanodia J. Time to rethink the current paradigm for assessing kidney function in drug development and beyond. *Clin Pharmacol Ther*. 2022;112(5):946–58.

Publisher's Note

Springer Nature remains neutral with regard to jurisdictional claims in published maps and institutional affiliations.